

X-ray Absorption Spectroscopy of Low Temperature Fuel Cell Catalysts

Andrea E. Russell* and Abigail Rose

School of Chemistry, University of Southampton, Highfield, Southampton SO17 1BJ, U.K.

Received December 16, 2003

Contents

1. Introduction	4613
2. X-ray Absorption Spectroscopy	4614
2.1. XANES	4614
2.2. EXAFS	4615
3. Data Collection and In Situ Cells	4618
4. XAS as a Characterization Method: Pt/C	4620
4.1. Particle Size	4620
4.2. Potential Dependence	4621
4.3. Adsorbates	4624
5. Pt Containing Alloy Catalysts	4626
5.1. PtRu Alloys	4627
5.1.1. Compositional Analysis	4628
5.1.2. Potential Dependence	4628
5.1.3. Adsorbates	4629
5.2. Other Pt Containing Alloy Anode Catalysts	4630
5.3. Pt Containing Alloy Cathode Catalysts	4630
6. Non-Pt Catalysts	4632
7. Conclusion	4633
8. References	4633

1. Introduction

In the last two decades X-ray absorption spectroscopy (XAS) has increasingly been applied to the study of fuel cell catalysts and, in particular, Pt containing catalysts for use in low temperature fuel cells. The increasing use of XAS may be attributed to its unique potential to provide information regarding the oxidation state and local coordination, numbers and identity of neighbors, of the absorbing atom. The advantage of XAS over other characterization methods, such as XPS or SEM/EDAX, lies in the ability to conduct the measurements in situ, in environments that closely mimic those of a working fuel cell.

In the application of XAS to the study of fuel cell catalysts, the limitations of the technique must also be acknowledged; the greatest of which is that XAS provides a bulk average characterization of the sample, on a per-atom basis, and catalyst materials used in low temperature fuel cells are intrinsically nonuniform in nature, characterized by a distribution of particle sizes, compositions, and morphologies. In addition, the electrochemical reactions of interest in fuel cells take place at the surface of catalyst par-

ticles, and XAS is not able to provide a means of directly probing the surface composition or electronic/chemical state of the surface of the catalyst particles. Throughout this review both the advantages and limitations of XAS in the characterization of low temperature fuel cell catalysts will be emphasized.

An XAS experiment measures the change in the absorbance, μx , or fluorescence of the sample as the X-ray energy is scanned through the absorption edge. At the absorption edge the energy of the incident X-ray photon is sufficient to excite a core level electron of the absorbing atom to unoccupied atomic or molecular orbitals. A typical XAS spectrum is shown in Figure 1. The absorption, μx , is defined by the Beer Lambert equation,

$$\mu x = \log(I_0/I_t) \quad (1)$$

where μ is the linear absorption coefficient, x is the sample thickness, I_0 is the intensity of the incident photons, and I_t is that of the transmitted photons. The region closest to the absorption edge has a structure that is characteristic of the local symmetry and electronic structure of the absorbing atom, which is commonly called the XANES, X-ray absorption near edge structure. The position of the absorption edge can provide information regarding the oxidation state of the absorber. The XANES region extends to approximately 50 eV above the absorption edge. At higher energies the energy of the incident X-ray photons is sufficient to excite a core electron of the absorber into the continuum producing a photoelectron with kinetic energy, E_k ,

$$E_k = h\nu - E_{\text{binding}} \quad (2)$$

The ejected photoelectron may be approximated by a spherical wave, which is backscattered by the neighboring atoms. The interference between the outgoing forward scattered, or ejected, photoelectron wave and the backscattered wave gives rise to an oscillation in the absorbance as a function of the energy of the incident photon. These oscillations, which may extend up to 1000 eV above the absorption edge, are called the EXAFS, extended X-ray absorption fine structure. Analysis of the EXAFS provides information regarding the identity of, distance to, and number of near neighboring atoms.

This review will focus on the applications of XAS in the characterization of low temperature fuel cell catalysts, in particular carbon supported Pt electrocatalysts, Pt containing alloys for use as anode and

* To whom correspondence should be addressed. Phone: +44 (0) 2380 593306. Fax: +44 (0) 2380 596805. E-mail: a.e.russell@soton.ac.uk.



Andrea E. Russell was born in California and grew up in Michigan. She obtained her B.S. degree in Chemistry from the University of Michigan, Ann Arbor in 1986 and her Ph.D. in Physical Analytical Chemistry from the University of Utah, Salt Lake City in 1989 working with B. Stanley Pons. She then went to work with William O'Grady at the U.S. Naval Research Laboratory in Washington, DC, where she first started working with synchrotron radiation. In 1991 she moved to the U.K. as a Lecturer at the University of Liverpool, moving in 1994 to the University of Newcastle upon Tyne and in 1997 to the University of Southampton, where she is now a Reader and a Member of the Electrochemistry and Surface Science Group. Her research interests are in the application of spectroscopic methods to further the understanding of structure/property relationships in electrochemistry and electrocatalysis. Full use of the electromagnetic spectrum is made, from the far-infrared through to hard X-rays.



Abigail Rose was raised in Somerset, England. She obtained her B.Sc. degree in Chemistry from the University of Southampton in 1998. She remained at Southampton, obtaining an M.Phil. in 1999 under the supervision of Jeremy Frey and a Ph.D. in Physical Chemistry in 2003 working with Andrea Russell. Her Ph.D. thesis work, funded by the EPSRC at Johnson Matthey, was on the applications of in situ EXAFS to the study of PEM fuel cell catalysts. Presently, she is working as a fuel cell scientist at Dstl, Porton Down, a U.K. Ministry of Defence research laboratory.

cathode catalysts, and, finally, non-Pt containing cathode catalysts. A discussion of the cells that have been used for in situ and gas treatment measurements will be presented. The type of information that can be derived from XAS studies of fuel cell catalysts will be illustrated, and the relevant XAS literature from 1982 to 2003 will be reviewed.

2. X-ray Absorption Spectroscopy

The details of the analysis of the XANES and EXAFS regions of the XAS spectra are beyond the scope of this review. However, as XAS is becoming a more "routine" tool for the study of fuel cell catalysts,

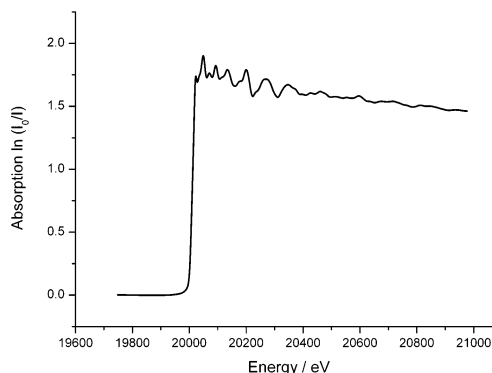


Figure 1. XAS spectrum of a Mo foil collected at the Mo K edge.

we feel that some discussion of the basic aspects of the analysis as applied to fuel cell catalysts is warranted and may assist the nonspecialist in understanding the origins of the information derived from XAS.

2.1. XANES

In the study of fuel cell catalysts, detailed analysis of the XANES region is not common. As mentioned in the Introduction, the position of the absorption edge is related to the oxidation state of the absorbing atom and the detailed features can provide an identification of the neighbors, coordination geometry, and, in the case of clusters of atoms, particle size and morphology. The XANES region of the XAS spectrum is dominated by multiple-scattering and multiphoton absorptions. As such, detailed analysis of this region is less straightforward than that of the EXAFS region, which will be described in section 2.2, and most studies have been limited to a so-called white line analysis, which will be discussed below. However, recent advances in the theoretical models and the availability of computer programs, such as the FEFF8 code developed by Rehr's group,¹ should encourage more detailed analysis of the XANES of supported metal catalysts.

The FEFF8 code is an *ab initio* code that implements a self-consistent, real-space Green's function approach. The recent improvements in the FEFF code are particularly apparent, in the analysis of L_{III} absorption edges, where transitions from the $2p_{3/2}$ level to vacant d-states of the absorbing atom occur. For example, Ankudinov and Rehr² have recently shown that the Pt L_{III} edge of a Pt foil is more reliably reproduced by the FEFF8 code, which is self-consistent, than by the FEFF7 code previously used by Bazin et al.³ The absorption coefficient and, therefore, intensity of the white line for a surface atom are not the same as those for a bulk atom, and this must be taken into account when fitting the XANES of nanoparticles, as demonstrated by Bazin et al. for Pt clusters of 13, 19, 43, and 55 atoms with the fcc structure (O_h symmetry).³ The morphology of the cluster was also shown to be important for Pt clusters⁴ and Cu clusters.⁵ Fitting the XANES data requires comparison of the spectrum to the spectra of a series of relevant reference compounds, which are then simulated using FEFF8. Detailed analysis

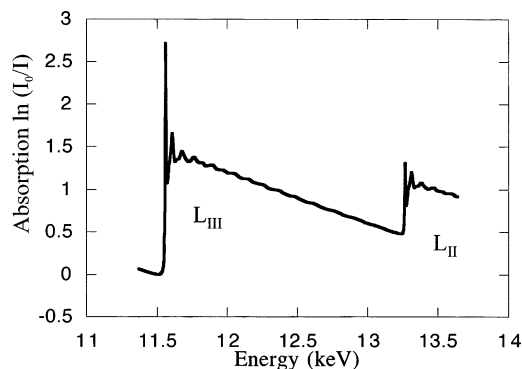


Figure 2. XAS spectrum of $\text{Na}_2\text{Pt}(\text{OH})_6$ powder.

of the XANES of a fuel cell catalyst, with a distribution of particle sizes and morphologies, can then be accomplished using principal component analysis (PCA). However, as noted by Bazin and Rehr,⁵ defining relevant reference compounds and the simulation of a large number of absorption spectra of possible structures, which may only contribute as minor components to the overall spectrum, are major limitations of this technique. However, the PCA-FEFF approach offers a real opportunity to obtain the distribution of the electronic states of catalyst particles.

The XANES region of the Pt L_{III} and L_{II} absorption edges can be used to determine the fractional d-electron occupancy of the Pt atoms in the catalyst sample by a so-called white line analysis. Figure 2 shows the XAS spectrum collected at both Pt L_{III} and L_{II} absorption edges of $\text{Na}_2\text{Pt}(\text{OH})_6$. The sharp features at the absorption edges are called white lines after the white line observed in early photographic film based XAS measurements.⁶ Mansour and co-workers⁷ have shown that comparison of the white line intensities of a sample with those of a reference metal foil provides a measure of the fractional d-electron vacancy, f_{d} , of the absorber atoms in the sample. f_{d} is defined as follows:

$$f_{\text{d}} = (\Delta A_3 + 1.11\Delta A_2)/(A_{3,\text{r}} + 1.11A_{2,\text{r}}) \quad (3)$$

where $A_{3,\text{r}}$ represents the area under the white line at the L_{III} edge and $A_{2,\text{r}}$ represents the area at the L_{II} edge of the reference foil spectrum and

$$\Delta A_x = A_{x,\text{s}} - A_{x,\text{r}} \quad (4)$$

with $x = 2$ or 3 and $A_{x,\text{s}}$ the area under the white line at the L_x edge of the sample spectrum. The areas may be determined by integration of the normalized (defined below) spectra from 10 eV below the absorption edge to 40 eV above the absorption edge or by first subtraction of an arc tangent function fit through the pre- and postabsorption edge regions.

f_{d} can then be used to calculate the total number of unoccupied d-states per Pt atom in the samples as follows:

$$(h_j)_{\text{t,s}} = (1.0 + f_{\text{d}})(h_j)_{\text{t,r}} \quad (5)$$

where $(h_j)_{\text{t,r}}$, t = total, for Pt has been shown to be 0.3.⁸ A large $(h_j)_{\text{t,s}}$ value, thus, indicates a smaller d-electron density and an increased d band vacancy

as compared to those for bulk Pt. Unfortunately, when $(h_j)_{\text{t,s}}$ values have been reported in the fuel cell literature, no estimation of the error in the measurement has been given. Therefore, it is best to treat the determination of $(h_j)_{\text{t,s}}$ as a semiquantitative measurement and to restrict its use to the comparison of relative values and the identification of trends.

2.2. EXAFS

To analyze the EXAFS region of the XAS spectrum, the raw data must first be subjected to background subtraction, determination of the zero point of the energy, and normalization. Background subtraction removes both the variation in the absorbance with energy caused by the other atoms in the sample (the near-linear variation seen before the edge, usually modeled as a modified Victoreen function⁹) and the smooth variation in μ past the absorption edge, corresponding to the absorption of the free atom. The zero point of the energy, E_0 , is usually taken as the inflection point in the absorption edge. This allows the energy of the incident photon, E_{hv} , to be converted to k -space (\AA^{-1}) as follows:

$$k = \left(\frac{2m_e}{\hbar} (E_{\text{hv}} - E_0) \right)^{1/2} \quad (6)$$

Normalization places the measured spectrum on a per-absorber-atom basis, thereby taking into account the concentration of the sample, and is division of the absorption data by the magnitude of the edge step at 50 eV above the absorption edge. The details of XAS data reduction may be found elsewhere.¹⁰

Once the EXAFS spectrum is isolated, the data may then be fitted to the EXAFS equation,

$$\chi(k) = \sum_{j=1}^{\text{shells}} A_j(k) \sin \delta_j(k) \quad (7)$$

with the amplitude function

$$A_j(k) = \frac{N_j}{kR_j^2} S_0^2 F_j(k) e^{-2k^2\sigma_j^2} e^{-2R_j/\lambda(k)} \quad (8)$$

and the phase function

$$\sin \delta(k) = \sin(2kR_j + \varphi_j(k)) \quad (9)$$

where N_j is the number of atoms of type j at the distance R_j from the absorber atom, $F_j(k)$ is the magnitude of the backscattering from atom j , $\delta_j(k)$ is the backscattering phase shift resulting from scattering off atom j , S_0 is the amplitude reduction factor and reflects multielectron effects and central atom shake-up and shake-off due to the relaxation process after photoionization, $e^{-2k^2\sigma_j^2}$ accounts for the finite lifetime of the excited state, σ_j^2 is the relative mean squared disorder along the distance between the absorbing atom and atom j due to thermal and static motions, and λ is the mean free path of the electron.

The backscattering amplitude, $F_j(k)$, and phase shift, $\delta_j(k)$, for the absorber-neighbor pair may be extracted from the EXAFS of reference compounds or calculated theoretically using widely available

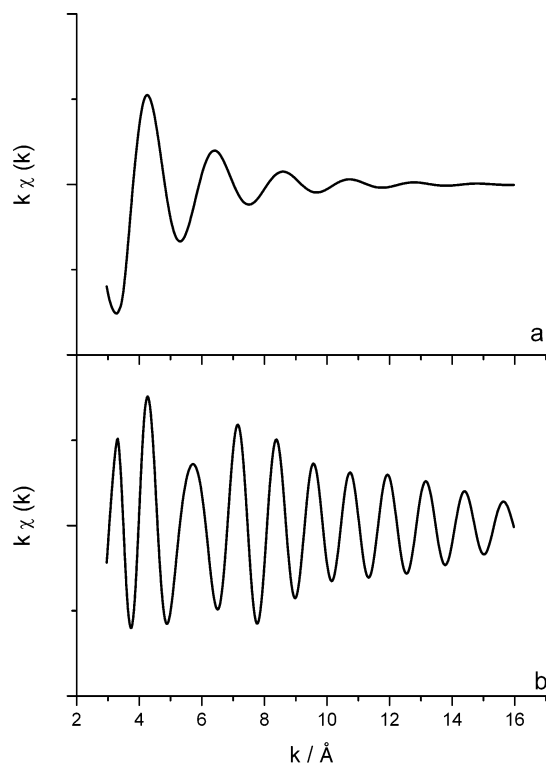


Figure 3. Calculated EXAFS of (a) Pt with six O neighbors at 1.98 Å and (b) Pt with six Pt neighbors at 2.77 Å.

programs such as the FEFF codes developed by John Rehr's group at the University of Washington.^{11–13} These parameters enable the identification of the neighbors surrounding the absorbing atom. In particular, the variation of the backscattering amplitude with energy, or k , provides an indication of the mass of the neighboring atom. The calculated EXAFS for Pt–O and Pt–Pt absorber–neighbor pairs are shown in Figure 3. As can be seen in the figure, the backscattering from a light neighbor, with low Z , is at a maximum at low k values and decays quickly, while that from a heavier neighbor, with high Z , extends to higher values of k . Weighting the EXAFS data from a sample with mixed neighbors by k or k^3 emphasizes the contributions to the EXAFS from the low and high Z neighbors, respectively. The coordination number, N_j , and the distance, R_j , also have easily visualized effects on the EXAFS. Increasing the number of a given type of neighbor increases the amplitude of the EXAFS, as shown in Figure 4 and eq 8. Variation of the near neighbor distance changes the phase of the EXAFS as shown in Figure 5 and eq 9. Attention to the effects of these parameters on the EXAFS can provide a useful starting point in fitting EXAFS data.

Fourier transformation of the EXAFS gives the radial structure function. The EXAFS and corresponding k^3 Fourier transform for a Pt foil standard are shown in Figure 6. As in the case of the raw EXAFS data, k weighting of the Fourier transformation emphasizes the contributions of low Z neighbors, k^1 weighting, or high Z neighbors, k^3 weighting. In the analysis of the EXAFS for a supported fuel cell catalyst, k^2 weighting of the Fourier transform is commonly used, as it provides a compromise, giving weight to the contributions from both low and high

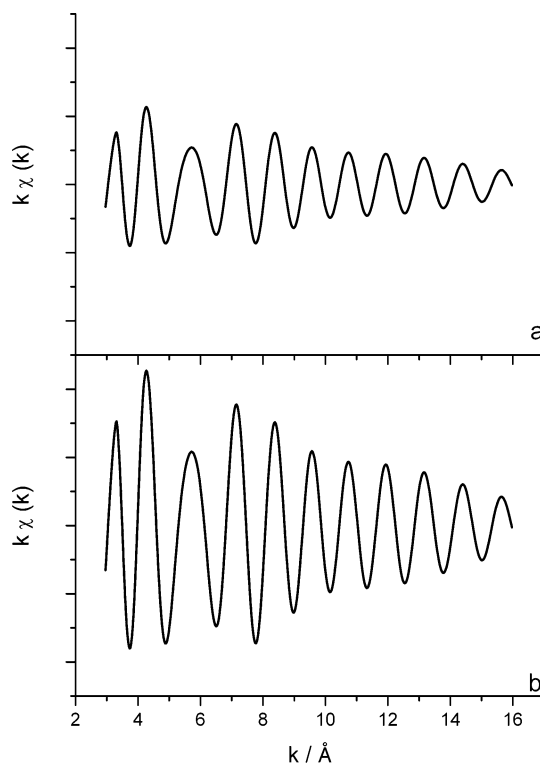


Figure 4. Calculated EXAFS of (a) Pt with six Pt neighbors and (b) Pt with 12 Pt neighbors at 2.77 Å.

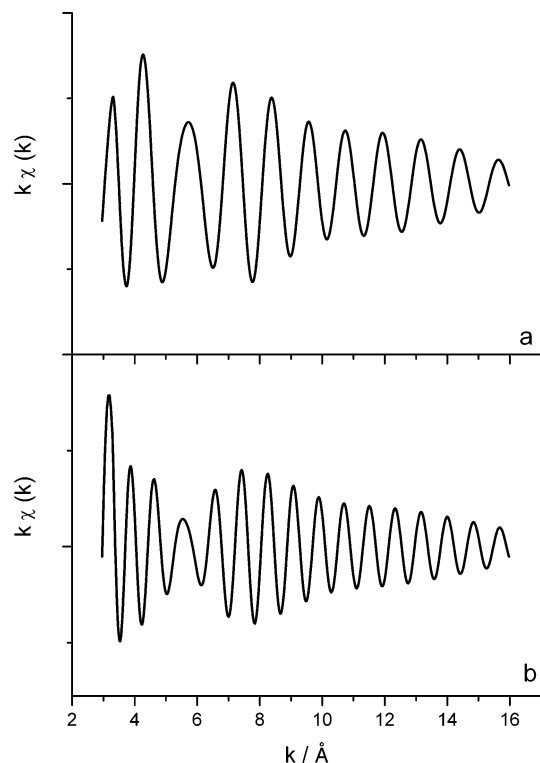


Figure 5. Calculated EXAFS of (a) Pt with six Pt neighbors at 2.77 Å and (b) Pt with six Pt neighbors at 3.42 Å.

Z neighbors. Phase correction of the Fourier transform by the backscattering phase shift of one of the absorber–neighbor pairs is also extensively used. This has the effect of correcting the distances observed in the radial structure function as well as emphasizing the contributions from the chosen ab-

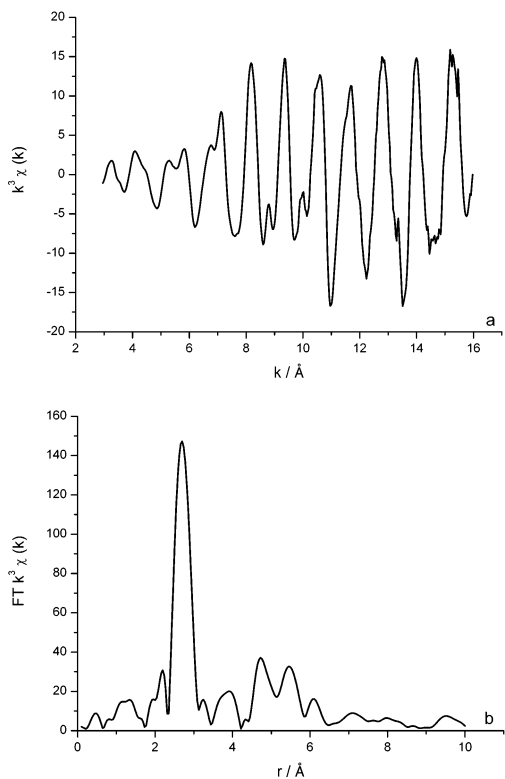


Figure 6. (a) k^3 weighted EXAFS of Pt foil collected at the Pt L_3 edge and (b) the corresponding k^3 weighted Pt phase corrected Fourier transform of the EXAFS data.

sorber–neighbor pair. Without phase correction the positions of the peaks in the radial structure function are all approximately 0.5 Å too short. The Fourier transform shown in Figure 6 corresponds to the radial structure of a Pt atom in the bulk fcc lattice, with 12 neighbors in the first shell, 6 in the second, 12 in the third, and 24 in the fourth. The decreased backscattering contribution from the neighbors at longer distances causes an apparent amplitude reduction of the radial structure function for higher shells, as predicted by eq 8.

EXAFS analysis involves fitting the data to the EXAFS equation to obtain a structural model. Currently, fitting EXAFS data relies on the user to propose candidate neighboring atoms as backscatters. The data are then fitted using the absorber–neighbor pairs. As such, the true applicability of the fits relies on chemical knowledge of the system under investigation obtained using other techniques.

There are many EXAFS analysis programs available, both commercial and free-ware, and the reader is referred to the web site of the International XAS Society for a comprehensive list.¹⁴ In preparing this review article, we found that three of these programs were much more commonly used than the others; the University of Washington UWXAFS package consisting of FEFF^{11–13} and FEFFIT, the Daresbury Laboratory code EXCURVE98 and its predecessor EXCURVE92, and the commercial program XDAP. As described previously, FEFF is a program for the ab initio calculation of phase shifts and effective backscattering amplitudes of single- and multiple-scattering XAFS and XANES spectra for clusters of atoms. There are several versions of FEFF available,

the most recent being FEFF7¹⁵ and FEFF8.¹ Versions of FEFF later than FEFF5, which included multiple-scattering paths, are equally appropriate for the provision of theoretical standards for EXAFS fitting; the improvements in the level of theory in versions 7 and 8 have more impact on the simulation of the XANES as discussed in section 2.1. The FEFFIT program fits the experimental EXAFS data to the theoretical standards calculated using FEFF in r -space and includes an estimate of the errors. EXCURVE98 is a combined theory and fitting program in which the backscattering phase shifts and amplitudes are calculated using rapid curved wave theory¹⁶ and the Rehr Albers theory^{11,12} from the parameters of the radial shells of atoms surrounding the absorber. The EXAFS data are fitted in k -space using least squares refinement, errors are estimated by calculation of the standard deviations of each parameter, and correlations between parameters may be examined. The theoretical standards generated using FEFF and EXCURVE98 can include multiple-scattering pathways. Inclusion of multiple scattering is important if higher coordination shells are to be included in the analysis, particularly those at distances equal to or greater than twice the distance to the first coordination shell. The XDAP program supplied by XSI makes use of both theoretical standards calculated using FEFF and/or experimentally derived backscattering phase shifts and amplitudes extracted from the EXAFS data of reference compounds collected by the user. The use of experimentally derived standards must be treated with caution and relies on the separation of EXAFS contributions from the various neighbors in the reference compound and the quality of the data. The EXAFS data may be fitted in k - or r -space using XDAP, and the program includes a subtraction facility which enables the difference file¹⁷ method to be easily implemented, as will be discussed below in section 4.3.

The errors in the fitting parameters may be obtained from the covariance matrix of the fit if it is available, but they are more commonly estimated by varying one parameter away from its optimal value while optimizing all other parameters until a defined increase in the statistical χ^2 function is obtained.¹⁸ However, the statistical error values obtained do not represent the true accuracies of the parameters. In fact, it is difficult to determine coordination numbers to much better than $\pm 5\%$,^{19,20} and $\pm 20\%$ is more realistic; when the data are collected at room temperature taking into account the strong coupling between the coordination number and Debye Waller terms, the error in the latter may be $\pm 30\%$.

The number of statistically justified free parameters, n , which may be fitted should also be taken into account when fitting the data. This may be estimated from the Nyquist theorem²¹ as follows:

$$n = \frac{2\Delta k \Delta r}{\pi} + 1 \quad (10)$$

where Δk and Δr are the ranges in k - and r -space over which there is useful data. This should not extend to regions where there are no meaningful data above the noise. For a data set with a Δk range of

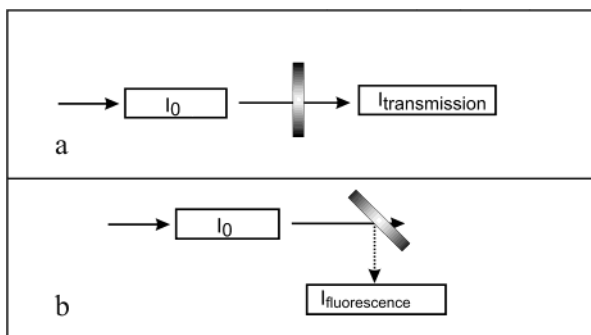


Figure 7. Experimental configuration for (a) transmission measurements and (b) fluorescence measurements. The sample is indicated by the shaded rectangle, I_0 and $I_{\text{transmission}}$ are ionization chamber detectors, and $I_{\text{fluorescence}}$ is a solid-state detector.

10 \AA^{-1} and an r -space interval of 2 \AA , application of the Nyquist theorem limits the free parameters to 14. Finally, the chemical feasibility of the fit should be examined. If the number of free parameters is not limited, it is possible to fit any EXAFS spectrum to a high level of apparent precision, and it is this observation that has given EXAFS a poor reputation in the past.

The IXAS also provides guidelines and standards for the publication of XAS data.^{22,23} In preparing this review, we found that many of the papers included did not adhere to these guidelines and standards, and while this did not invalidate the findings of most of the affected papers, it was occasionally difficult to assess the quality of the data and fits. A common omission was a statistical measure of the goodness of the fit. This may be defined as

$$R_{\text{EXAFS}} = \left\{ \sum_i^N \frac{1}{\sigma_i^{\text{exp}}} (|\chi_i^{\text{exp}} - \chi_i^{\text{th}}|) \right\} \times 100\% \quad (11)$$

where N is the total number of data points, σ^{exp} is the standard deviation for each data point, i , and χ^{exp} and χ^{th} are the experimental and theoretical EXAFS, respectively, although other definitions may be used. It is also expected that at least one representative EXAFS spectrum and the corresponding Fourier transform will be shown with the fit superimposed.

3. Data Collection and in Situ Cells

XAS measurements require a radiation source that is both intense and tunable, and therefore, they are usually conducted using synchrotron radiation. The measurements may be made using either transmission or fluorescence. The former is the more simple but is not suitable for dilute samples where fluorescence is more sensitive. A typical experimental configuration for a transmission measurement is shown in Figure 7. The intensity of the X-rays is monitored before and after the sample, I and I_0 , respectively, using ionization chamber detectors. The thickness or amount of the sample is selected to give an optimal change in the absorbance from one side of the absorption edge to the other in the range 0.3–1.0. The total absorbance of the sample at a given wavelength can be calculated from the X-ray absorp-

tion cross sections of all the elements²⁴ in the sample. The total absorbance of the sample and any other cell components in the X-ray beam path, such as windows or solution layers, should be kept to less than 2.5 to provide the best data quality. A reference metal foil or sample containing the element of interest and a third ionization chamber may be included to provide an internal standard for energy calibration. A full spectrum takes between 20 and 60 min to collect using a conventional scanning monochromator. The data collection time can be reduced to minutes by using a Quick EXAFS monochromator or even seconds if an energy dispersive monochromator is used.^{25–27} The former uses a microstepper to continuously scan the angle of the monochromator crystals, thereby reducing the dead time, and the latter uses a monochromator with a bent crystal to obtain the spectrum in a single exposure on a position sensitive solid-state detector. Unfortunately, a reduction in the quality of the EXAFS data collected usually accompanies any reduction in the collection time.

The experimental configuration for fluorescence measurements is shown in Figure 7. As in the case of transmission measurements, the intensity of the X-rays before the sample is measured using an ionization chamber. The sample is set at 45° to the path of the incident X-rays, so that the maximum solid angle of the fluorescence may be collected at the solid-state detector.

The XAS spectrum provides information regarding the average oxidation state and local coordination of the absorbing element. It is therefore crucially important when designing in situ cells for XAS measurements that complete conversion, electrochemical or chemical, of the material takes place.²⁸ XAS data of fuel cell catalysts may be obtained using samples prepared from the catalyst powders, PTFE or Nafion bound electrodes, or membrane electrode assemblies. Where the catalyst powders are studied, these are often made into pellets diluted with either boron nitride, silica, or polyethylene powder to aid preparation of the pressed pellet, similar to a potassium bromide pellet used in infrared spectroscopy. These particular diluents are chosen because they are composed of low Z elements and, therefore, are transparent at most X-ray energies. A gas treatment cell, such as that shown in Figure 8, has been used to collect the XAS spectra of self-supporting pellets of catalyst powders exposed to gas mixtures at elevated temperatures; the data are collected at either room or liquid nitrogen temperature.^{29,30} The pellet must be permeable to the gas mixture, and therefore, boron nitride was used as the diluent.

A number of designs of transmission in situ XAS cells have been published for the study of bound catalyst electrodes.^{31–33} These cells all utilize a thin-layer geometry to minimize the contribution to the absorbance by electrolyte solution. The cell design reported by McBreen and co-workers³¹ shown in Figure 9 uses three layers of filter paper soaked in the electrolyte as a separator, or later a Nafion membrane³⁴ between the working electrode and a Grafoil counter electrode. Bubbles in the electrolyte, that would result in noise in the XAS data, are

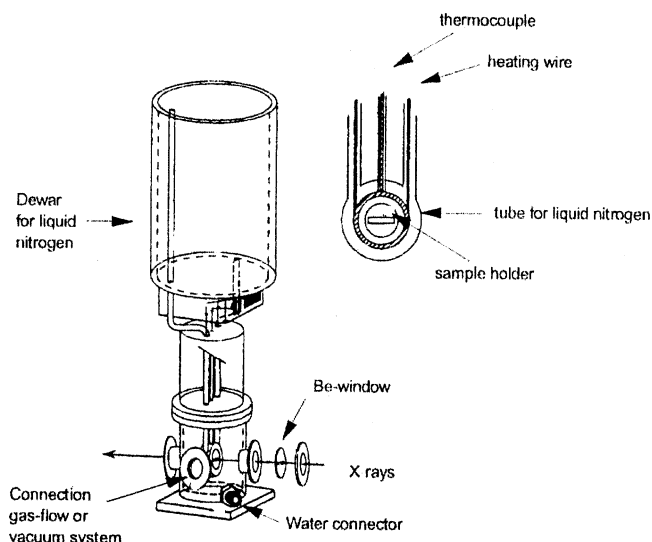


Figure 8. Gas treatment cell for transmission XAS.¹⁵⁴ The sample is prepared as a pressed self-supporting pellet in the sample holder, diluted with BN. The liquid nitrogen dewar enables data collection at 77 K, and the connection to gas-flow or a vacuum system enables control of the sample environment. (Reproduced with permission from ref 154. Copyright 1997 B. L. Mojet).

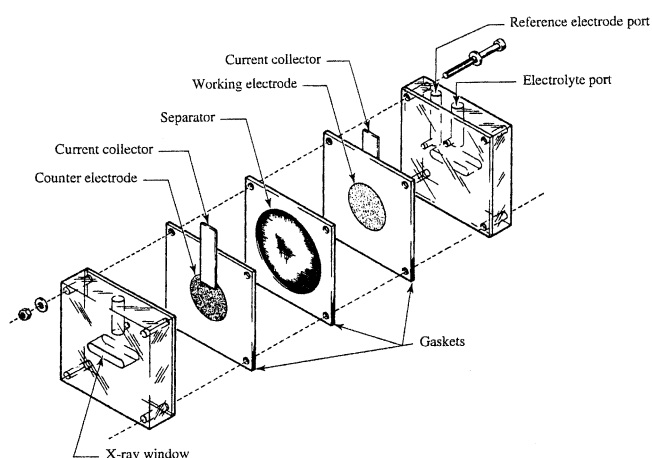


Figure 9. Electrochemical cell for transmission XAS.³¹ (Reproduced with permission from ref 31. Copyright 1987 American Chemical Society.)

prevented by keeping the entire assembly under compression.³⁵ Herron et al.³² also used filter papers as a separator between the working electrode and a gold foil counter electrode (Figure 10) but relied on continuously pumping electrolyte through the cell to sweep out any bubbles, as did the modified design described by Maniguet, Mathew, and Russell,³³ shown in Figure 11. In the former a hole was in the center of the gold foil counter electrode through which the X-rays passed, and in the latter the platinum gauze counter electrode was contained in a concentric electrolyte filled channel outside the path of the X-rays.

Collection of in situ XAS data using a single cell fuel cell avoids problems associated with bubble formation found in liquid electrolytes as well as questions regarding the influence of adsorption of ions from the supporting electrolyte. However, the in situ study of membrane electrode assemblies (MEAs) in a fuel cell environment using transmission

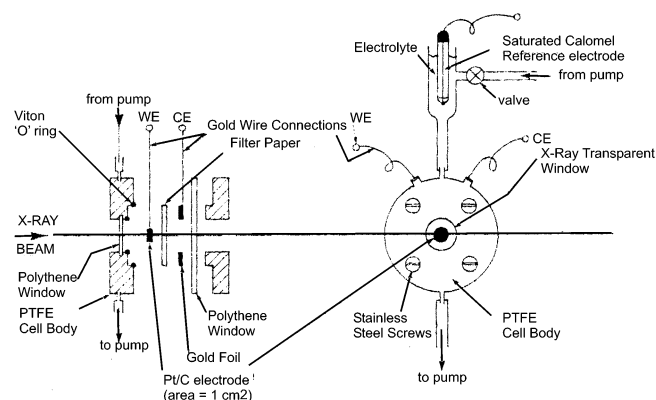


Figure 10. Electrochemical cell for transmission XAS.³² (Reproduced with permission from ref 32. Copyright 1992 Elsevier Sequoia S.A., Lausanne.)

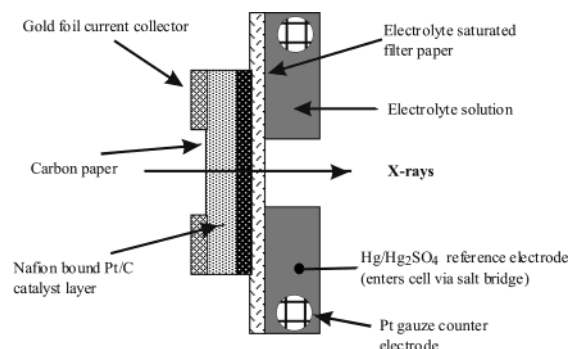


Figure 11. Electrochemical cell for transmission XAS.³³ (Reproduced with permission from ref 33. Copyright 2000 American Chemical Society.)

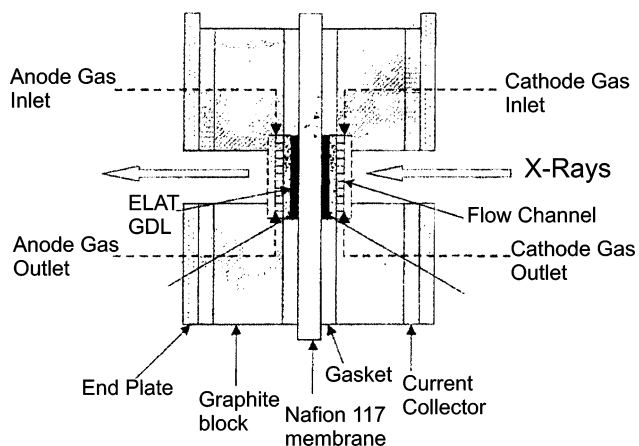


Figure 12. Fuel cell modified for transmission XAS.³⁷ (Reproduced with permission from ref 37. Copyright 2002 American Chemical Society.)

EXAFS requires either removal of the catalyst from the side of the MEA not under investigation³⁶ or exclusion of the absorbing element from this electrode.³⁷ The cell design reported by Viswanathan and co-workers³⁷ shown in Figure 12 is a modification of a single fuel cell. The graphite blocks on each side of the cell containing the flow channels for the gases were thinned to 2 mm to provide a path for the X-ray beam. To avoid problems with sampling the catalysts on both the anode and cathode sides of the MEA, they have replaced the cathode ink with Pd/C. In contrast, the cell design reported by Roth and co-workers³⁶ had a small portion of the Pt/C cathode catalyst removed

to allow investigation of the PtRu/C anode catalyst. This removal of the cathode catalyst in the beam window may modify the current distribution in the region of the anode catalyst probed by the X-rays, and therefore, correlation of the XAS spectra with simultaneously obtained electrochemical measurements may be of limited value.

4. XAS as a Characterization Method: Pt/C

As described above, XAS measurements can provide a wealth of information regarding the local structure and electronic state of the dispersed metal particles that form the active sites in low temperature fuel cell catalysts. The catalysts most widely studied using XAS have been Pt nanoparticles supported on high surface area carbon powders,^{25,27,29,30,32,33,38–52} represented as Pt/C. The XAS literature related to Pt/C has been reviewed previously.^{25,35} In this section of the review presented here, the Pt/C system will be used to illustrate the use of XAS in characterizing fuel cell catalysts.

4.1. Particle Size

The catalysts used in low temperature fuel cells are usually based on small Pt particles dispersed on a carbon support with typical particle sizes in the range 1–10 nm in diameter. The XAS provides a measure of the average electronic state and local coordination of the absorbing atom, for example, Pt, on a per-atom basis, as described above. Thus, the XAS, for both the XANES and EXAFS regions, of such Pt/C catalysts reflects the size of the particles.

The effect of particle size on the XANES region of the XAS spectra for Pt/C catalysts has been investigated by Yoshitake et al.³⁹ and Mukerjee and McBreen.⁴⁶ Figure 13 shows the XANES region as a function of the applied potential at the Pt L₃ edge for 3.7 and ≤1.0 nm diameter particles. The white line intensity increased for both particle sizes as the potential was increased, but the extent of the change was greater for the smaller particles. As described above, the white line intensity at the Pt L₃ and L₂ edges can be used to calculate an average fractional d-electron occupancy, f_d , of the Pt atoms in the particle. The lower white line intensity at negative potentials thus corresponds to a more metallic state. The effect of particle size at the most negative

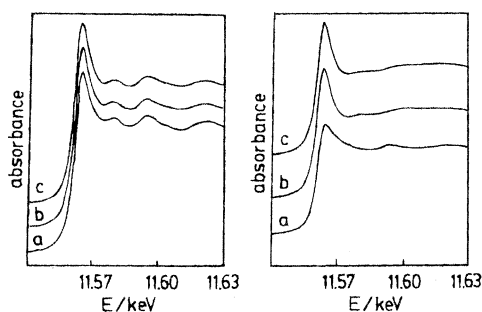


Figure 13. Pt L₃ XANES of 4 wt % Pt/C electrodes (left, 3.7 nm diameter particles; right, <1.0 nm diameter particles) at (a) -0.2 V, (b) 0.5 V, and (c) 1.0 V vs SSCE.³⁹ (Reproduced with permission from ref 39. Copyright 1994 The Electrochemical Society, Inc.)

Table 1. Calculated Values of the Effect of Particle Size on the Fraction of Atoms on the Surface and First Shell Coordination Numbers (CN) for Cuboctahedron (N_{cuboct}) and Icosahedron (N_{icos}) Models for Pt Clusters³¹

Pt loading/ wt %	avg particle size from XRD analysis/Å	surface fraction $N_{\text{surf}}/N_{\text{total}}$	first shell CN	
			N_{cuboct}	N_{icos}
20	30	0.39	10.35	10.62
30	40	0.28	10.87	11.05
40	53	0.24	11.06	11.22
60	90	0.15	11.45	11.54

potential, -0.2 V vs Ag/AgCl, is opposite that found for Pt particles supported on alumina, where a larger f_d value (greater white line intensity) was found for smaller particles. Yoshitake and coauthors attributed this difference to the formation of metal–hydrogen bonds in the electrochemical environment. The smaller particles have a greater fraction of the Pt atoms at the surface that are able to form such bonds. Mukerjee and McBreen⁴⁶ examined this in more detail later and noted that the XANES region for Pt/C catalysts at potentials where hydrogen is adsorbed exhibited widening on the high energy side of the white line peak. Such widening was compared to that previously reported by Mansour et al.^{53,54} and Samant and Boudart⁵⁵ for oxide supported Pt catalyst particles and attributed to the transitions into unoccupied antibonding Pt–H orbitals near the Fermi level.

The effects of particle size on f_d were further investigated by Mukerjee and McBreen.⁴⁶ f_d values were calculated for Pt/C particles with four different diameters at potentials corresponding to the hydrogen adsorption, 0.0 V vs RHE, the double layer, 0.54 V vs RHE, and the oxide formation, 0.84 V vs RHE, regions. Their results are summarized in Table 1. The calculated values show an increased widening of the white line with decreasing particle size at 0.0 V, little effect of particle size at 0.54 V, and an increase in the white line intensity at 0.84 V. The latter was attributed to the adsorption of oxygenated species, and in particular OH. When the change in f_d on going from 0.0 to 0.54 V and then from 0.54 to 0.84 V is normalized by dividing by the fraction of Pt atoms that are at the surface of the particle, as shown in Figure 14, it is apparent that the electronic effects of H and OH adsorption remain greater for the smaller particles. This increased effect was attributed to stronger adsorption of both H and OH on the smaller particles. The intrinsic activity of carbon supported Pt particles for the oxygen reduction reaction, ORR, in acidic solutions has been shown to depend on both the shape and size of the particles,^{56,57} with increased activity observed for larger particles. At the larger particles, the decreased strength of adsorption of OH leaves more of the surface available to take part in the ORR, summarized as the $(1 - \Theta)$ effect in the recent review by Markovic and Ross.⁵⁸

The effects of particle size on the EXAFS region of the XAS spectra are reflected in the coordination numbers obtained in the fits to the EXAFS data. Figure 15 shows the EXAFS or $\chi(k)$ data and corresponding Fourier transforms for a Pt foil, a PtO₂

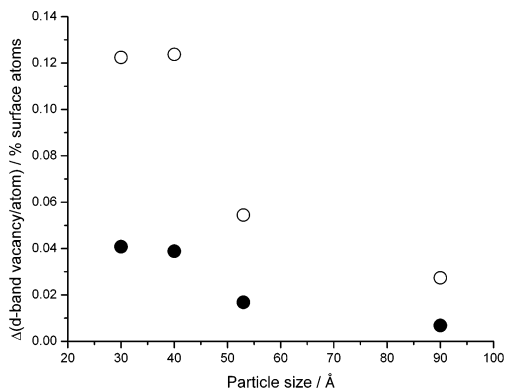


Figure 14. Effect of average particle size on the change in normalized d band vacancies (d band vacancies/% surface atoms) (filled circles) on going from 0.54 to 0.0 V vs RHE and on going from 0.54 to 0.84 V (open circles). (Adapted from ref 31 with permission. Copyright 1998 Elsevier Sequoia S.A., Lausanne.)

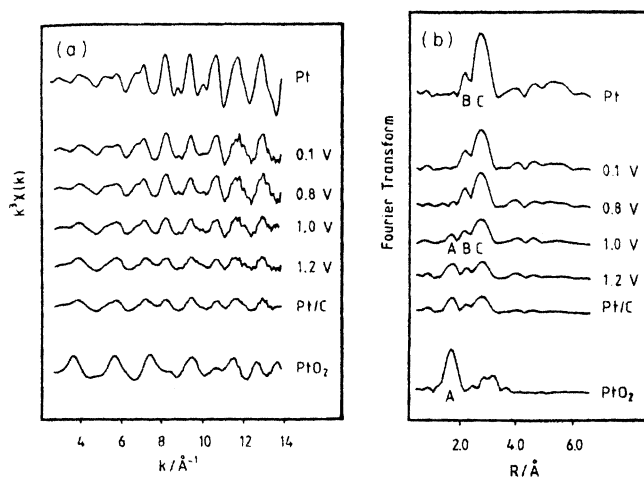


Figure 15. k^3 weighted experimental Pt L_3 EXAFS (a) and corresponding Fourier transforms (b) of Pt foil, a 20 wt % Pt/C electrode at 0.1, 0.8, 1.0, and 1.2 V vs SCE, a dry Pt/C electrode, and a PtO_2 reference sample.³² (Reproduced with permission from ref 32. Copyright 1992 Elsevier Sequoia S.A., Lausanne.)

reference compound, and a Pt/C catalyst electrode. The reduced amplitude of both the EXAFS oscillations and the peak in the Fourier transform at 3.0 Å for the Pt/C electrode compared to that obtained for the Pt foil is a consequence of the smaller number of Pt neighbors at this distance. Bulk Pt metal is fcc, and the first shell coordination number is 12. For small particles, the average first shell coordination number is reduced, as the atoms on the particle surface do not have the full number of neighbors. Benfield⁵⁹ has derived analytical formulas for the number of atoms and average first shell coordination numbers for icosahedron and cuboctahedron clusters with complete shells of atoms. Figure 16 shows the icosahedron and cuboctahedron with 147 atoms formed when four complete shells are present. Benfield's formulas have been used in the interpretation of the EXAFS parameters obtained for supported metal particles to estimate the average particle size. However, these formulas are only valid for icosahedra and cuboctahedra with complete shells. If the outermost shell is incomplete, or can be represented as adatoms on a complete shell, the average particle size

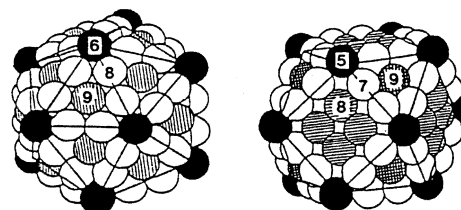


Figure 16. Icosahedron (left) and cuboctahedron (right) with 147 atoms corresponding to four complete shells. The numbers indicate the first shell coordination numbers of the surface atom sites.⁵⁹ (Reproduced with permission from ref 59. Copyright 1992 Royal Society of Chemistry.)

predicted from the first shell coordination number will be smaller than the actual particle size. The presence of incomplete shells and/or deviations from icosahedral or cuboctahedral particle shapes accounts for the observation that the average particle sizes predicted using the first shell coordination numbers obtained from EXAFS are usually smaller than those obtained from TEM measurements of the same catalysts. In addition, the EXAFS measurements represent the per-atom average of all the absorber atoms in the sample and, therefore, include particles too small to be observed using TEM.

4.2. Potential Dependence

The effect of the applied potential on the XANES region of the XAS spectra for Pt/C catalysts has been briefly introduced above and is related to both the adsorption of H at negative potentials and the formation of the oxide at more positive potentials. The adsorption of H and the formation of oxides are also apparent in the EXAFS and corresponding Fourier transforms, as seen in the work by Herron et al.³² shown in Figure 15. As the potential is increased from 0.1 to 1.2 V vs SCE, the amplitude of the peak in the Fourier transform at 2.8 Å decreases and that at 1.8 Å increases. The effect on the EXAFS, $\chi(k)$, data is less easily observed; the amplitude of the oscillations at $k \geq 8 \text{ Å}^{-1}$ decreases as the potential is increased, with the greatest change seen between 0.8 and 1.0 V. The results of fitting these data are shown in Table 2. Note that a value for the inner potential

Table 2. Structural Parameters^a Obtained from Best Least-Squares Fits of the EXAFS for the 20 wt % Pt/C Catalyst Electrode for Various Potentials, E^{17}

E/V vs SCE	atom	N	$r/\text{Å}$	$2\sigma^2/\text{Å}^2$
0.1	Pt	7.5	2.76	0.012
	Pt	2.6	3.90	0.017
	Pt	13.0	4.74	0.026
0.8	O	0.8	2.07	0.012
	Pt	6.4	2.76	0.012
	Pt	3.3	3.90	0.017
1.0	Pt	10.3	4.75	0.026
	O	1.8	2.07	0.013
	Pt	4.7	2.76	0.012
1.2	Pt	2.3	3.89	0.017
	Pt	7.1	4.75	0.026
	O	2.8	2.05	0.013
	Pt	2.9	2.76	0.013
	Pt	1.9	3.91	0.017
	Pt	4.6	4.75	0.026

^a N is the coordination number, r is the neighbor shell distance, and $2\sigma^2$ is the structural disorder term.

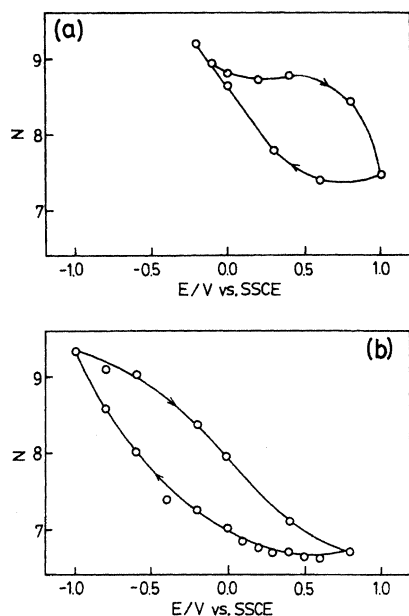


Figure 17. Coordination number of the first Pt–Pt shell for 4 wt % Pt/C electrodes in (a) $0.25 \text{ mol dm}^{-3} \text{ H}_2\text{SO}_4$ and (b) $1 \text{ mol dm}^{-3} \text{ NaOH}$ as a function of the applied potential.⁴⁰ (Reproduced with permission from ref 40. Copyright 1993 Elsevier Sequoia S.A., Lausanne.)

correction, ΔE_0 , was not given in this paper. In the hydrogen adsorption region, at 0.1 V, there are 7.5 first shell Pt neighbors at 2.76 \AA and no O neighbors, corresponding to a well reduced particle. As the potential is increased and the particle becomes oxidized, the first shell Pt neighbors are replaced by O neighbors, eventually reaching 2.8 O neighbors at 2.05 \AA and 2.9 Pt neighbors at 2.75 \AA at 1.2 V. The number of Pt neighbors at longer distances or in higher coordination shells also decreases as the potential is increased. However, the fcc shell structure of bulk Pt is maintained, thereby indicating that only a thin oxide is formed on the particle surface, the thickness of which increases with increasing potential. Yoshitake et al.⁴⁰ have shown that, upon reversing the direction of the potential sweep, a hysteresis in the first shell Pt coordination number is observed. The results can be plotted in a manner similar to a voltammogram and are shown in Figure 17 for a Pt/C electrode in either $0.2 \text{ mol dm}^{-3} \text{ H}_2\text{SO}_4$ or $1 \text{ mol dm}^{-3} \text{ NaOH}$.

Combining the EXAFS results with the potential variation of the white line intensity or f_d , a schematic model of the potential dependent structure of the carbon supported Pt particles has been proposed by Yoshitake et al.⁴⁰ and this model is shown in Figure 18. The effect of increasing the potential in the oxide region is both to grow an oxide film on the surface of the particle and to roughen the particle surface. Upon reversing the potential sweep to remove the oxide, this roughness remains until hydrogen is adsorbed on the particle surface. The influence of adsorbed hydrogen on the first shell Pt coordination number has also been reported by Mukerjee and McBreen,⁶⁰ who compared the EXAFSs of Pt/C catalysts at 0.0 and 0.54 V vs RHE, corresponding to the adsorbed hydrogen and double layer regions, respectively. A decrease in the coordination number was observed

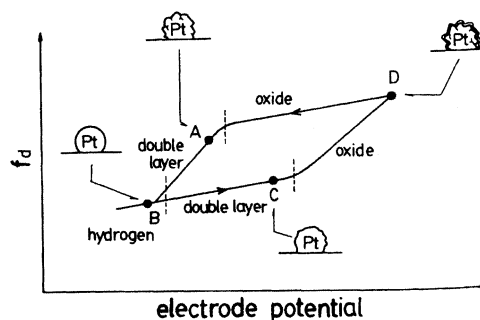


Figure 18. Schematic model of the structure of Pt particles on an f_d voltammogram in relation to the electrode potential. The hydrogen, double layer, and oxide regions are based on cyclic voltammetry. The lattice disorder decreases in the order $D > A > C > B$.⁴⁰ (Reproduced with permission from ref 40. Copyright 1993 Elsevier Sequoia S.A., Lausanne.)

upon increasing the potential, for example, from 10.56 to 8.66 for a 30 \AA particle. They proposed that this change indicated a change in the particle morphology from a sphere at 0.0 V to a flatter raftlike structure at 0.54 V.⁴⁶

The rate of oxide formation and/or removal at Pt/C electrodes has been investigated using energy dispersive EXAFS (EDE) by several authors.^{25,27,40,43,61} In EDE the conventional double crystal, scanning monochromator is replaced by a bent crystal dispersive or Laue monochromator, enabling data over a range of X-ray energies to be collected simultaneously. The transmitted X-rays are monitored using a position sensitive detector, and thus, an entire XAS spectrum can be collected as a single snapshot in as little as 1 s. More recent developments in detector technology may improve the data collection rate to the millisecond time scale,⁶² however, they have not yet been applied to the study of fuel cell electrocatalysts. The rate of oxide formation or removal is measured by monitoring the change in either the first shell Pt or O coordination numbers, N_{Pt} or N_{O} , as a function of time either following a potential step or during a cyclic voltammogram. Figure 19 shows the Fourier transforms as a function of time obtained following a potential step from 0.1 to 1.2 V vs RHE for the oxide formation and back for oxide reduction reported by Allen and co-workers.⁴³ The EXAFS data were fitted and N_{Pt} and N_{O} are shown as a function of time after the potential step in Figure 20. The oxide formation measured as an increase in N_{O} and the absorption peak or white line intensity or a decrease in N_{Pt} was best fit with a logarithmic function with all three indicators changing at the same rate. In contrast, the oxide reduction kinetics were best modeled as a single-exponential function, with different rate constants for the loss of N_{O} and the growth of N_{Pt} . This difference is clearly seen in Figure 20B as a delay between the changes in N_{O} and N_{Pt} . The results highlight an interesting difference between the mechanisms of oxide formation on bulk Pt, which occurs by a place exchange mechanism to form ordered PtO_2 ,^{63–65} and that occurring at small Pt particles. The authors proposed a model of oxide formation at small particles invoking the contrasting driving forces of the formation of Pt–O bonds and

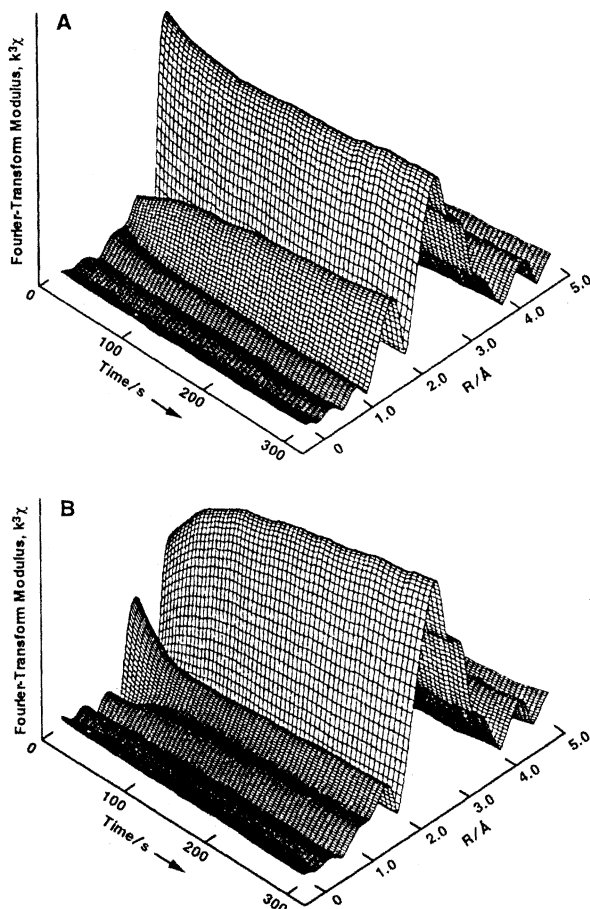


Figure 19. Fourier transform of the Pt L₃ EXAFS acquired during (A) the oxidation and (B) the reduction of a carbon supported Pt catalyst electrode as a function of time. Note that the Fourier transforms have not been phase corrected. The peak at 2.24 Å corresponds to the first shell of Pt near neighbors at 2.76 Å. The peak at 1.50 Å is a combination of the side-lobe from the Pt shell and a shell of O near neighbors at 2.01 Å.⁴³ (Reproduced with permission from ref 43. Copyright 1995 Elsevier Sequoia S.A., Lausanne.)

the minimization of the total surface area of the particle, which has the effect of Pt–Pt restructuring.

O'Grady and co-workers^{47,66} have shown that an additional potential dependent feature may be identified as a low frequency oscillation in the XAS spectrum, which yields peaks in the Fourier transform of the data at values of r (Å) which are too small to be realistically attributed to scattering of the photoelectron off near neighbor atoms.⁶⁷ This phenomenon, termed the atomic X-ray absorption fine structure or AXAFS, is attributed to scattering of the photoelectron by the interstitial charge density around the absorbing atom.⁶⁸ The AXAFS oscillations, $\chi_e(k)$, are superimposed on the background absorption of the free atom, $\mu_a(E)$, giving structure to the atomic absorption, $\mu_0(E)$, as follows.

$$\mu_0(E) = \mu_a(E)[1 + \chi_a(E)] \quad (12)$$

These oscillations are usually removed from the EXAFS, $\chi(k)$, data during the background subtraction process according to eq 12, as previously they were

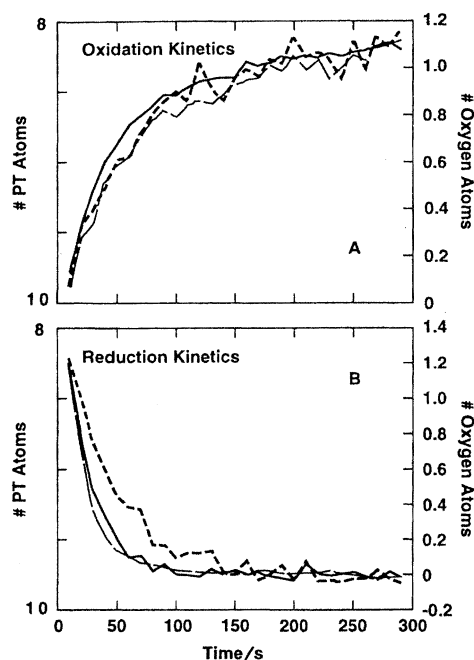


Figure 20. Structural parameters as a function of time extracted by fitting the data shown in Figure 20. (A) Data collected during the oxidation of the Pt/C electrode and (B) during the reduction: long dashes, first shell O coordination number (no. of O atoms); short dashes, first shell Pt coordination number (no. of Pt atoms); solid line, absorption peak intensity (effectively white line intensity).⁴³ (Reproduced with permission from ref 43. Copyright 1995 Elsevier Sequoia S.A., Lausanne.)

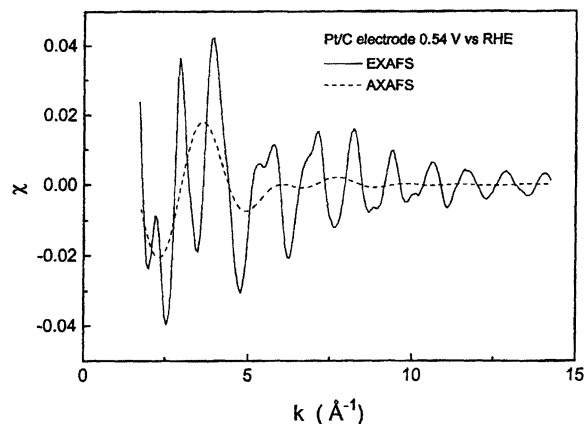


Figure 21. Experimental Pt L₃ EXAFS data for a Pt/C electrode at 0.5 V vs RHE (solid line) and the back transformed Fourier filtered AXAFS signal (dotted line). Fourier filtering parameters: $0.5 \leq k \leq 8.5 \text{ \AA}^{-1}$ and $0.15 \leq r \leq 1.7 \text{ \AA}$.⁴⁷ (Reproduced with permission from ref 47. Copyright 1998 Elsevier Sequoia S.A., Lausanne.)

not thought to have a fundamental interpretation.

$$\chi(k) = \frac{\mu(k) - \mu_0(k)}{\mu_0(k)} \quad (13)$$

The background removal procedure has been modified by O'Grady et al.⁴⁷ to retain the AXAFS in the EXAFS data. Figure 21 shows the EXAFS of a Pt/C electrode at 0.54 V vs RHE obtained using such a background removal procedure and the isolated AXAFS obtained by applying a Fourier filter in the low r (Å) range. The authors show that the amplitude

of the AXAFS is dependent on the applied electrode potential, increasing as the potential is changed from 0.00 to 0.54 V and then to 0.74 V. Using the FEFF7 code^{69,70} and performing calculations for a Pt₁₃ cluster, they show that the variations in the amplitude of the AXAFS observed can be modeled by including a charge of ± 0.05 e per surface Pt atom. This interpretation is, however, somewhat controversial. The FEFF codes utilize a muffin-tin approximation to the atomic potentials of the absorber and back-scattering atoms. The potentials are assumed to be spherical within the muffin-tin radius and zero outside, which corresponds to the interstitial region. O'Grady and Ramaker⁴⁷ have modified the point of the cutoff between these two potential regions to reproduce the AXAFS features. Such a modification does not overcome any inherent errors in the muffin-tin approximation. It should also be noted that the Fourier filtering range chosen by O'Grady and Ramaker, $0.5 \text{ \AA}^{-1} \leq k \leq 8.5 \text{ \AA}^{-1}$ and $0.15 \text{ \AA} \leq r \leq 1.7 \text{ \AA}$, overlaps with any tail from the peak in the Fourier transform from oxygen neighbors and, therefore, the variations in the AXAFS observed may simply be related to the presence of oxygen neighbors at the higher potentials. Finally, there does not exist a general agreement regarding the physical origins of AXAFS features. Other phenomena such as multi-electron excitations that will influence the shape of the XAS spectrum in the near-edge region must also be considered.⁷¹

4.3. Adsorbates

As described in previous sections, the adsorption of hydrogen and oxide formation at Pt/C electrocatalysts are apparent in both the XANES and EXAFS regions of the spectrum collected at the Pt L₃ edge. XAS spectra are normalized to a per-atom basis, and therefore, the impact of an adsorbate on the spectrum collected at the Pt L₃ edge, or any other Pt edges, will depend on the fraction of the Pt atoms located at the surface of the particle or the dispersion. For typical Pt/C electrocatalyst particles in the 1–5 nm range, the dispersion is 0.6–0.2. The coordination number, N_X , obtained from the EXAFS corresponding to a full monolayer of an adsorbate, X, that did not cause restructuring of the particle, would only be 0.6–0.2. (The larger coordination numbers associated with oxide formation, N_O , therefore, provide evidence of restructuring of the metal particle, as discussed previously.) Such low coordination numbers are smaller than the errors normally associated with fitting the EXAFS data. Collecting the XAS data at an absorption edge associated with the adsorbate and ensuring that any excess of the adsorbate is removed from the sample prior to collection of the XAS data may improve the reliability of the parameters associated with Pt–adsorbate bonds. This method has been used to investigate the underpotential deposition (upd) of Cu,^{72,73} Pb,⁷⁴ and Rb⁷⁵ on Pt/C electrocatalysts. The upd of Cu on Pt/C is described below as an example.

McBreen and co-workers have investigated the upd of Cu from $0.5 \text{ mol dm}^{-3} \text{ H}_2\text{SO}_4 + 4 \times 10^{-4} \text{ mol dm}^{-3} \text{ CuSO}_4$ on to Pt/C, examining both the XANES⁷³ and

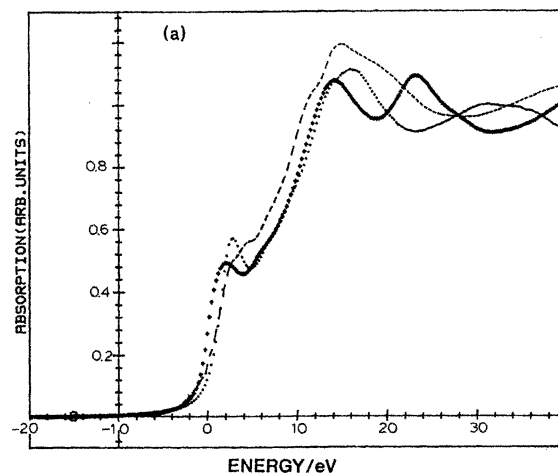


Figure 22. Normalized Cu K XANES for Cu foil (+), Cu₂O (dots), and upd Cu on Pt/C at 0.05 V vs SCE (dashes).⁷³ (Reproduced with permission from ref 73. Copyright 1991 Elsevier Sequoia S.A., Lausanne.)

EXAFS⁷² regions at the Cu K and Pt L₃ absorption edges. To minimize the contributions of Cu species in the electrolyte solution, most of the electrolyte was drained from the cell. Electrochemical control of the Pt/C working electrode was maintained by keeping a small portion of the electrode in contact with the remaining solution. Oxygen was carefully excluded from the drained cell to avoid competing Faradaic processes and to maintain the upd layer. Figure 22 shows the normalized XANES for Cu foil and Cu₂O reference samples as well as that of the Cu upd layer. The edge position for the upd Cu layer was shown to correspond to Cu⁺, and the shape of the edge supported a tetrahedral coordination. At the Pt L₃ edge a slight decrease in the white intensity was observed, corresponding to charge transfer to the Pt upon adsorption of Cu. When the Cu K edge EXAFS data were later examined,⁷² the fitting supported a tetrahedral coordination of the Cu atoms with 1 Pt neighbor at 2.68 Å and 3 O neighbors at 2.06 Å. An additional S neighbor at 2.37 Å was required to reproduce the apparent splitting of the first shell peak in the Fourier transform, as shown in Figure 23. The S neighbor was accounted for by including a coadsorbed SO₄²⁻ anion. The observed splitting of the peak in the Fourier transform was attributed to interference effects between the backscattering from the O and S neighbors. This observation highlights the danger in simply interpreting peaks in the Fourier transforms of EXAFS data as neighbors at the distance indicated by the position of the peaks; in this case neighbors at approximately 1.4, 2.2, and 2.8 Å would have been anticipated. Subsequent surface X-ray scattering measurements of Cu upd on Pt(111) single-crystal surfaces^{76–78} have confirmed the coadsorption of Cu and HSO₄⁺ but disagree with the assignment of the oxidation state of the Cu as +1; rather, the Cu is thought to be uncharged or only slightly positively charged.

In the investigation of adsorbed species using XAS, it is not always possible to probe adsorbate–substrate bonding by changing to the adsorption edge of the adsorbate, for example, the adsorption of carbon monoxide on carbon supported Pt particles. Carbon

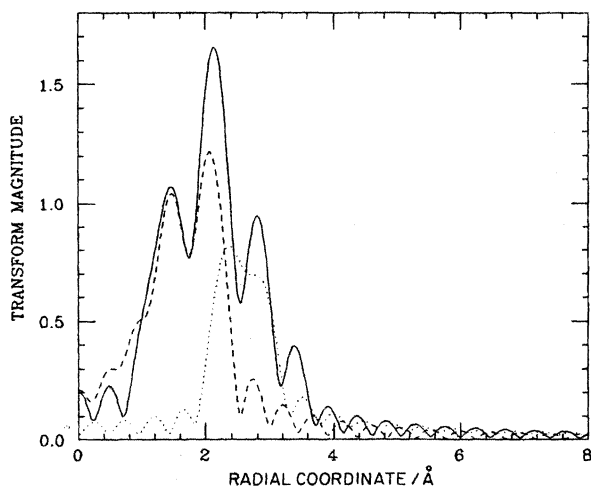


Figure 23. Breakdown of the combined Cu–O and Cu–S contribution (dashed line) and the Cu–Pt contribution (dotted line) to the Fourier transform of the Cu K edge data obtained for an upd layer of Cu on Pt/C at 0.05 V vs SCE.⁷² (Note: Radial coordinate/Å is the same as $R/\text{Å}$.) (Reproduced with permission from ref 72. Copyright 1993 Elsevier Sequoia S.A., Lausanne.)

monoxide adsorption is of particular interest in low temperature fuel cells, as it may be present in the H_2 feed produced by re-forming hydrocarbons and is also a partial oxidation product of methanol, used as the anode feed in the direct methanol fuel cell. The presence of carbon in the support as well as the large background absorption at the C K edge by the other elements present in the fuel cell catalyst and electrolyte preclude investigation at the C K edge. Maniguet et al.³³ have shown that the use of a difference file method¹⁷ to separate the various contributions to the EXAFS obtained at the Pt L_3 edge enables the in situ investigation of the adsorption of CO on Pt/C electrocatalyst electrodes. The difference file method as applied to the CO adsorption on Pt/C may be briefly described as fitting the dominant Pt–Pt contributions to the EXAFS data and then subtracting this fit from the data. The remaining, weaker, Pt–C and/or Pt–O contributions could then be fit. These weaker contributions were then subtracted from the original data and the Pt–Pt contributions refit. The cycle was repeated several times until no further variation in the parameters was observed. Figure 24 shows the Fourier transforms of the isolated Pt–Pt contributions and the

combined Pt–C and Pt–O contributions at 0.05 V vs RHE with adsorbed CO; 1.05 V, where the Pt/C particles are oxidized; and 0.45 V, after the CO has been electrochemically removed from the Pt/C surface. A peak attributed to Pt–C of adsorbed CO is observed at approximately 1.5 Å in Figure 24a and the fit yielded 0.5 C neighbors at a distance of 1.85 Å attributed to linearly adsorbed CO. The other peaks in Figure 24(a) and those in 24(c) were attributed to C neighbors of the support as previously reported by Lampitt et al.³⁰ and O’Grady and Koningsberger.²⁹ These neighbors are present in the EXAFS of all C supported catalyst particles, but are only evident when the dominant contributions from the metal neighbors are removed and are, therefore, not usually included in the fitting. The Fourier transform of the non-Pt contributions at 1.05 V is dominated by O neighbors as anticipated following the onset of oxide formation.

Additional contributions to the EXAFS from the O of the adsorbed CO will have been present in the data presented by Maniguet et al.³³ but were not fitted. For linearly adsorbed CO the collinear or near collinear arrangement of Pt–C≡O enhances the contributions of this multiple-scattering pathway to the EXAFS. Thus, as previously reported for $\text{Os}_3(\text{CO})_{12}$ adsorbed on $\gamma\text{-Al}_2\text{O}_3$ ¹⁷ and $\text{Pt}_2\text{Ru}_4(\text{CO})_{18}$ adsorbed on $\gamma\text{-Al}_2\text{O}_3$,⁷⁹ the O neighbor of the CO ligands could easily be observed in the EXAFS obtained at the Os and Pt and Ru edges, respectively. However, the presence of a large number of Pt neighbors at a similar distance in the case of the Pt/C catalyst dominates the EXAFS data reported by Maniguet et al., masking the contributions of the O neighbors of the adsorbed CO.

The adsorptions of H, O, and SO_4^{2-} on Pt/C electrocatalyst electrodes have been further investigated by O’Grady and Ramaker^{48–51} by comparing the XANES data at the Pt L_2 and L_3 absorption edges. In their analysis, the difference spectrum, which they term AS for antibonding state, is obtained as follows:

$$\text{AS} = \Delta L_3 - \Delta L_2 \quad (14)$$

where ΔL_n is the difference spectrum at the L_n edge between the Pt/C electrode at a reference potential and the potential of interest. The theory behind the subtraction method is that the L_3 edge contains

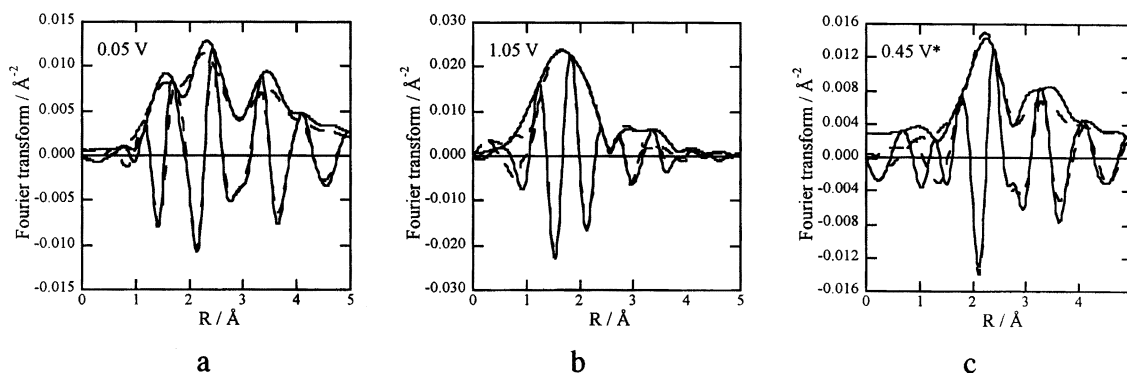


Figure 24. Fourier transforms of the isolated non-Pt contributions to the Pt L_3 EXAFS of a 40 wt % Pt/C electrode at (a) 0.05 V vs RHE, with CO adsorbate present, (b) 1.05 V, with the Pt surface oxidized, and (c) 0.45 V after removal of CO and reduction of oxide.³³ (Reproduced with permission from ref 33. Copyright 2000 American Chemical Society.)

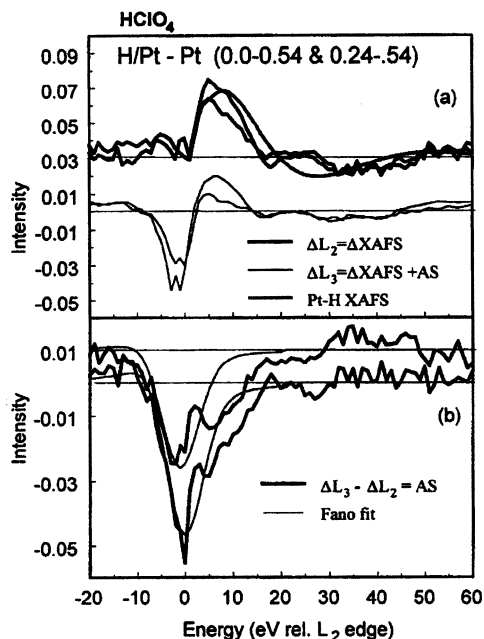


Figure 25. Comparison of the difference spectra for hydrogen adsorbed on Pt/C and Pt/C (0.0–0.54 V and 0.24–0.54 V), for a Pt/C electrode in 1 mol dm⁻³ HClO₄.⁴⁹ (Reproduced with permission from *Journal of Synchrotron Radiation* (<http://journals.iucr.org/>), ref 49. Copyright 1999 International Union of Crystallography.)

contributions from both the 2p_{3/2} to 5d_{3/2} and 5d_{5/2} transitions, while the L₂ edge corresponds to the 2p_{1/2} to 5d_{3/2} transition. Any antibonding orbitals (AS) formed upon adsorption will only contribute to the L₃ spectrum, because at the L₂ edge spin-orbit coupling causes the AS to be nearly filled. Thus, the difference between the XANES data at the L₃ and L₂ edges will represent the valence band density of states probed at the L₃ edge. By first taking the difference between the spectrum at the L_n edge at the potential of interest and a reference potential, and then obtaining the spectrum AS, any observed features should be attributable to changes in the valence band and the formation of any additional antibonding states above the valence band brought about by the change in the applied potential. The antibonding state formed is degenerate with the continuum and, therefore, is a “shape” resonance, which will have a characteristic Fano-resonance line shape.

The Pt L_{2,3} difference spectra for a Pt/C electrode at 0.0 and 0.24 V vs RHE and the reference potential of 0.54 V are shown as an example in Figure 25. In Figure 25a the calculated XAFS for Pt–H is also included and seen to agree with the ΔL₂ spectrum as well as the ΔL₃ spectrum at energies greater than 5 eV relative to the L₂ edge. The remaining features in the ΔL₃ spectrum at lower energies are more clearly seen in the AS spectrum (Figure 25b). The physical origins of the features in the AS spectra are not clear from the papers published thus far, and the detailed interpretation is beyond the scope of this review. The Fano fit shown in Figure 25b is characterized by a resonance energy which is negative for potentials where H is adsorbed, 0.0 and 0.24 V vs RHE, and positive where O is adsorbed, 1.14 V. This

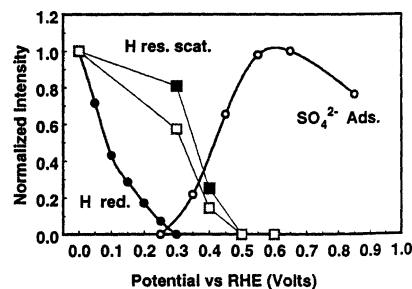


Figure 26. Comparison of the resonance scattering from H atoms or H⁺ obtained by fitting the Fano line shape in HClO₄ (open squares) and H₂SO₄ (closed squares) with the adsorbed hydrogen coverage (closed circles) and sulfate adsorption (open circles) obtained by cyclic voltammetry.⁵⁰ (Reproduced with permission from ref 50. Copyright 2001 The Electrochemical Society, Inc.)

resonance energy has been shown to vary with the size of the metal cluster and becomes more negative as the cluster becomes more metallic.⁸⁰ Thus, the more positive resonance energy at 1.14 V is in agreement with other data showing that the particles are oxidized at this potential.

In Figure 26 the amplitude of the peak in the AS spectrum is plotted as a function of the potential for a Pt/C electrode in 0.5 mol dm⁻³ H₂SO₄ and 1.0 mol dm⁻³ HClO₄. The amplitude of the peak is related to the resonant scattering from H and, therefore, provides a measure of the extent of H adsorption. The offset between the H coverage derived from the electrochemical measurements (filled circles) and that from the AS peak amplitude (squares) has been interpreted as suggesting that hydrogen, as H⁺, does not fully leave the Pt surface until the potential reaches 0.4 V vs RHE and that when the H⁺ leaves the surface, SO₄²⁻ ions are directly adsorbed.⁵⁰ This unexpected result indicates that use of this L_{2,3} difference method may provide new insights regarding adsorption on Pt/C. However, the method cannot be generally applied to other metals of interest as fuel cell catalysts, as it relies on the accessibility of the L₃ and L₂ absorption edges.

5. Pt Containing Alloy Catalysts

XAS is particularly useful in the investigation of alloy electrocatalysts. Unlike XRD measurements, which only reflect the crystalline component of the sample, and TEM, which is limited to particles with diameters greater than 1 nm, XAS provides the average local structure surrounding all of the atoms of the absorbing element in the sample. By collecting the XAS data at the absorption edges corresponding to each element in the alloy under investigation, the extent of intermixing and homogeneity of the alloy may be assessed. It is generally accepted that surface segregation, which is the enrichment of one element in the surface relative to the bulk, is common in bimetallic alloys; see, for example, the review by Campbell⁸¹ and the comments by Markovic and Ross in their recent review.⁵⁸ XAS provides an indirect probe of the surface composition of the catalyst particles, by comparison of the coordination numbers obtained in fitting the data at each absorption edge.

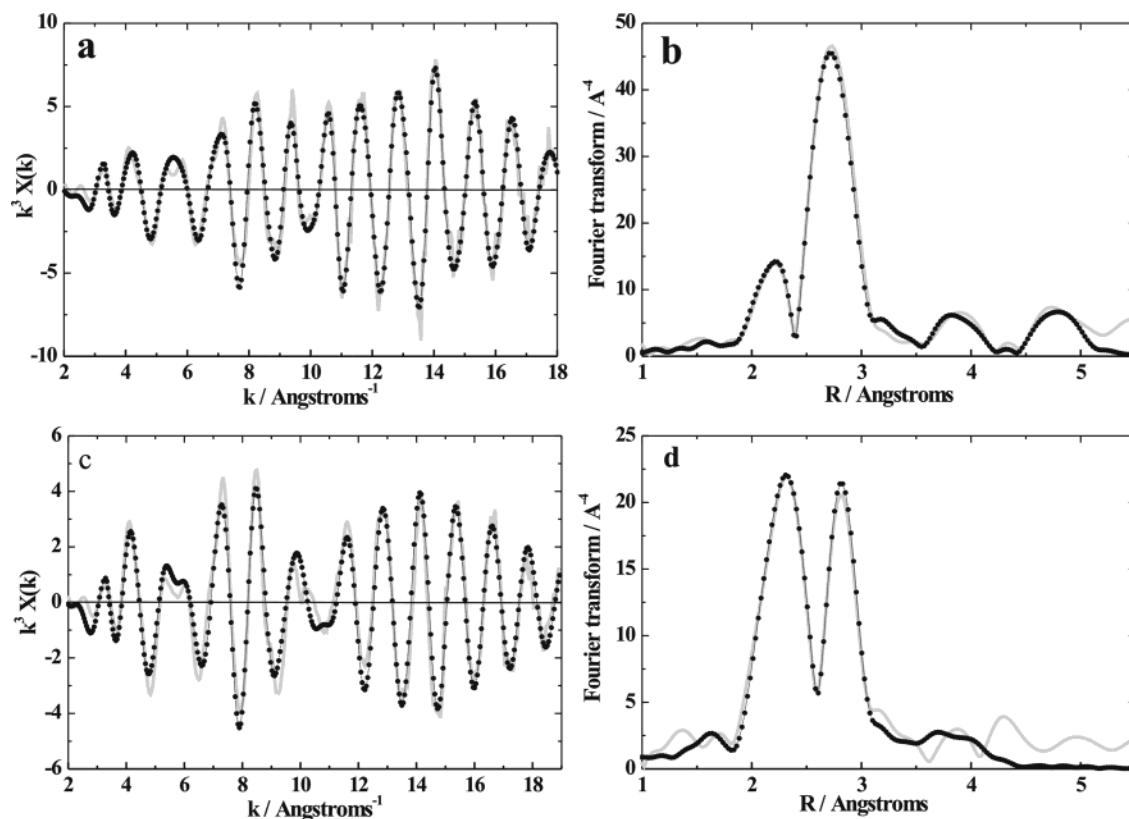


Figure 27. k^3 weighted Pt L_3 EXAFS (a and c) and the corresponding Fourier transforms (b and d) for (a and b) a poorly mixed PtRu/C alloy electrode and (c and d) a well mixed PtRu/C alloy electrode at 0.05 V vs RHE in 1 mol dm^{-3} H_2SO_4 ; experimental data (solid line) and fits (dotted line).⁸⁷ (Reproduced with permission from ref 87. Copyright 2002 S. Maniguet.)

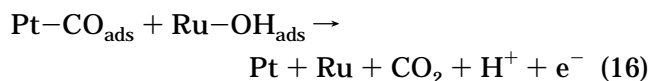
In addition, as described extensively above, the XAS data can be collected in situ and, thereby, enable the investigation of the stability of the alloy system.

The alloy catalysts used in low temperature fuel cells are usually based on Pt. Anode catalysts are sought that have improved tolerance to the presence of carbon monoxide in the reformat derived hydrogen feed for PEM fuel cells or better long term performance for methanol oxidation for direct methanol fuel cells. Cathode alloy catalysts should have enhanced oxygen reduction kinetics and/or tolerance to methanol crossover. Much of our current knowledge regarding the role of secondary, or even ternary, elements in enhancing the electrocatalytic activity of Pt containing electrocatalysts has been derived from studies on well characterized single-crystal electrode surfaces, as summarized in the excellent review by Markovic and Ross.⁵⁸ However, in advancing our understanding of real electrocatalysts, an understanding of the structure of supported nanoparticle catalysts is invaluable. In this section of the review structural investigations of Pt containing alloy catalysts will be presented.

5.1. PtRu Alloys

PtRu alloys are well-known for both their improved CO tolerance^{82–85} and improved methanol oxidation⁸⁶ as compared to the case of Pt. The enhanced behavior of PtRu over Pt has been attributed to a bifunctional

mechanism⁸⁴ (see eqs 14 and 15 below) in which the



Ru provides sites for water activation as well as having an electronic effect on the Pt atoms, such that CO is less strongly adsorbed. In situ XAS measurements have been used to determine the structure of PtRu catalysts, to assess the magnitude of any electronic effect that alloy formation may have on the Pt component of the catalyst, and to provide evidence in support of the bifunctional mechanism.

The analysis of the EXAFS of alloy catalyst particles is inherently more complicated than that of single metals. In the case of PtRu catalysts there is an added complication that the backscattering from Pt and Ru neighbors at similar distances interfere with one another, giving rise to beats in the EXAFS data. This phenomenon was first described by McBreen and Mukerjee⁶⁰ for a poorly alloyed 1:1 atomic ratio PtRu/C catalyst. The presence of beats in the EXAFS data is more apparent in the EXAFS obtained at the Pt L_3 edge for a well mixed 1:1 PtRu/C catalyst than in that of a poorly mixed catalyst of the same composition,⁸⁷ as shown in Figure 27; compare panels a and c. Pandya et al.⁸⁸ showed that the beats occur because the difference in the backscattering phase shifts from Pt and Ru is

approximately π radians in the range $6 \text{ \AA}^{-1} < k < 11 \text{ \AA}^{-1}$, giving rise to destructive interference between the Pt–Pt and Pt–Ru contributions in the EXAFS at the Pt edge. A similar effect is observed at the Ru K edge.⁸⁷ The presence of such beats causes an apparent splitting of the peak corresponding to the first coordination shell in the Fourier transform of the data. In the past, such data were analyzed by constraining some of the analysis parameters, and Fourier filtering to isolate the EXAFS for the first coordination shell was frequently used. Advances in the computer programs used in the fitting and the use of theoretical backscattering phase shifts and amplitudes have meant that such techniques are no longer necessary and the data may be fit as shown in Figure 27, where EXCURVE98^{16,89} was used.

5.1.1. Compositional Analysis

The extent of intermixing of PtRu catalysts has been investigated using EXAFS by a number of authors.^{60,87,90} As shown in Figure 27, the splitting of the first shell peak in the Fourier transform is greater for a well mixed 1:1 PtRu alloy catalyst than for the poorly mixed catalyst. The difference in the extent of intermixing of these two catalysts was confirmed by fitting the data obtained at the Pt L_{III} and Ru K absorption edges. In the case of the well mixed alloy, the coordination environments seen from the Pt and Ru edges were in excellent agreement (same coordination numbers and distances of Pt–Ru and Ru–Pt), while, for the poorly mixed alloy, the Ru edge data showed that much of the Ru was present as an oxide (Ru–O neighbors present and fewer Pt–Ru and Ru–Pt neighbors than predicted by the 1:1 Pt:Ru composition). In fitting the EXAFS data obtained at two edges for such bimetallic particles, it is possible to restrict the number of adjustable parameters by ensuring that the distance between the two metal neighbors and the Debye Waller term for this shell are the same at both edges, as recommended by Meitzner et al.⁹¹ and recently applied by Alexeev and co-workers⁷⁹ in an EXAFS investigation of the structure of Pt–Ru carbonyl clusters on γ -Al₂O₃.

In a similar analysis, comparing the coordination numbers for first shell Pt and Ru neighbors obtained in situ in 1 mol dm⁻³ HClO₄ at the Pt L₃ and Ru K edges at 0.0 V vs RHE, McBreen and Mukerjee were able to estimate that only 10% of the Ru in the commercial catalyst they were investigating was alloyed with the Pt.⁶⁰ Examination of the Ru K edge data showed that the local structure of the Ru corresponded to a Ru oxide, RuO_x, with a Ru–Ru distance of 2.66 Å and a Ru–O distance of 2.02 Å, without any need to include Pt neighbors. Page et al.⁹² have obtained Pt EXAFS for a commercial 1:1 PtRu catalyst and found that the first coordination shell contained only Pt neighbors. They assumed that the structure of the PtRu particles could be best described as an onion, with Pt on the inside and Ru in an outer shell. However, without any evidence of Pt–Ru near neighbor interactions in the EXAFS or Ru K edge data, such an assumption is difficult to justify, and it is more likely that the Ru is present

as a separate oxide phase, as reported by McBreen and Mukerjee.⁶⁰ In addition, these authors report a first shell coordination number of 13.8 for a Pt foil and similar values for the PtRu catalysts when the parameter was allowed to vary, indicating that the analysis package used⁹³ produced suspect results.

Neto and co-workers examined the ex situ Pt L₃ EXAFS for a series of PtRu catalyst powders in air of varying nominal composition from 90:10 through to 60:40 atom %.⁹⁴ The catalysts were prepared using a formic acid reduction method developed by the authors which resulted in very poorly alloyed particles, even after heat treatment to 300 °C under a hydrogen atmosphere. Unfortunately, the authors were not able to obtain Ru K edge data to identify the local structure of the Ru in their catalysts.

Nashner et al.^{95,96} ensured that the average composition of the carbon supported PtRu particles they investigated was PtRu₅ by dispersing a molecular carbonyl cluster, PtRu₅C(CO)₁₆, on to a carbon support followed by reduction with hydrogen. EXAFS analysis of catalyst powders under a H₂ atmosphere at the Pt and Ru edges confirmed that alloy particles were formed and that the local coordination surrounding the Ru atoms contained only Pt and Ru. Comparison of the parameters obtained at the Pt and Ru edges showed that the distribution of the Pt and Ru neighbors in the particles was nonstatistical and could best be described by a segregation of Pt to the surface of the particle.

5.1.2. Potential Dependence

The applied electrode potential has been shown to have an effect on both the XANES and EXAFS of PtRu catalysts. The variations of the Pt d band vacancy per atom, $(h_j)_{t,s}$, with potential over the range 0.0–0.54 V vs RHE for both the poorly mixed 1:1 PtRu/C catalyst investigated by McBreen and Mukerjee⁶⁰ and a well mixed 1:1 PtRu/C catalyst studied by Russell et al.⁹⁷ were less than that for a pure Pt/C catalyst.⁹⁴ McBreen and Mukerjee attributed this difference to a reduction in the adsorption of hydrogen on the Pt sites of the alloy catalyst. The results also provide evidence of an electronic effect upon alloying Pt with Ru. The effects on the Ru XANES were much less significant, but some evidence of a change to a higher oxidation state at potentials above 0.8 V was observed.^{60,98}

For data collected at the Pt L₃ edge, increasing the potential from the hydrogen adsorption region to the double layer region, and subsequently to potentials corresponding to oxide formation at the metal particles, has been shown to be accompanied by a decrease in the total number of first shell metal neighbors, $N_{Pt} + N_{Ru}$.^{60,87,99} McBreen and Mukerjee also reported a slight change in the first shell Pt–Pt bond distance that they claimed provided evidence of a relaxation of the Pt–Ru bonding and subsequent restructuring of the PtRu particle. However, the magnitude of the variation reported, $2.72 \pm 0.01 \text{ \AA}$, was very small and may well be within the experimental error. O'Grady et al.⁹⁹ noted that while no Pt–O neighbors were present in the Pt L₃ data collected at 0.8 V vs RHE, Ru–O neighbors were

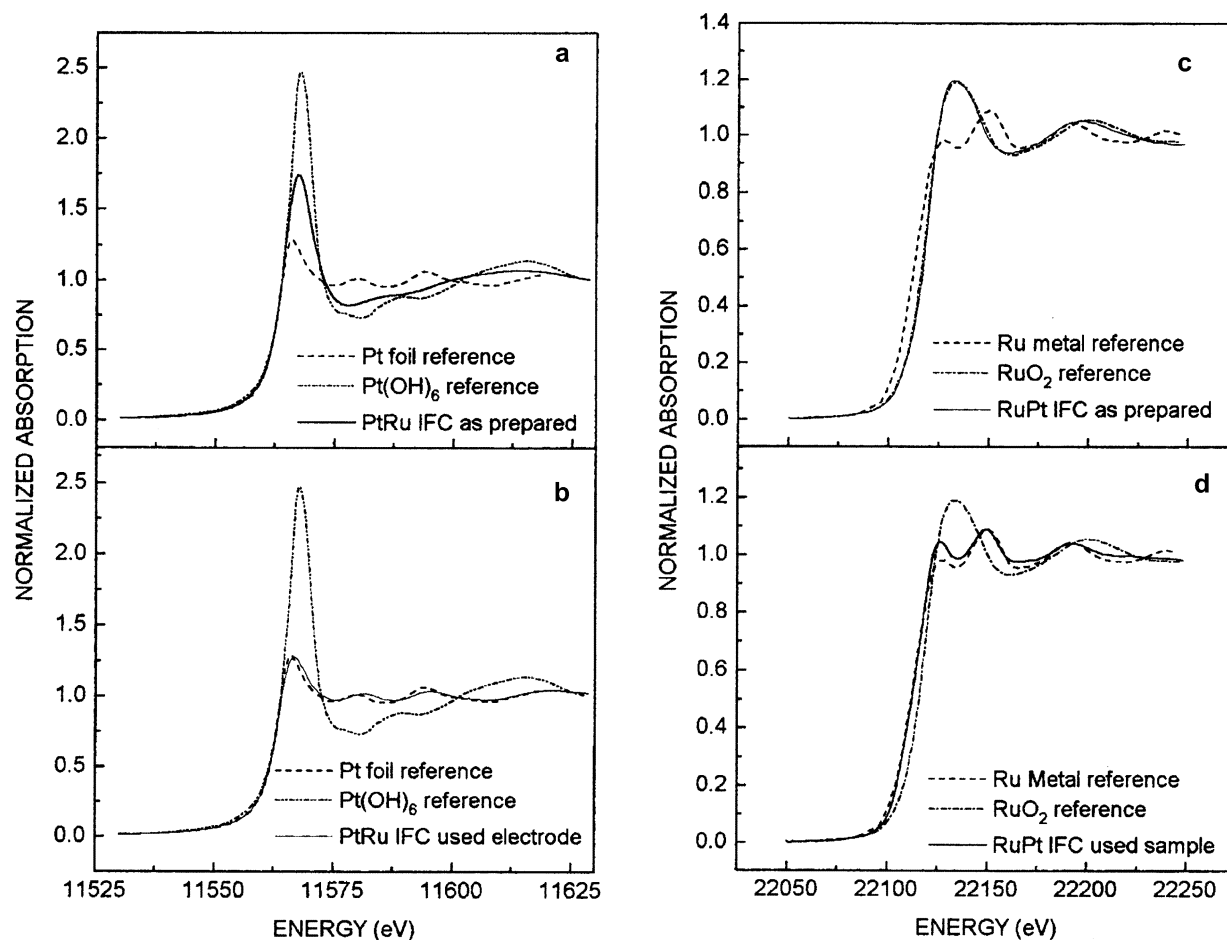


Figure 28. XANES for an unsupported PtRu black catalyst (a and c) as prepared and (b and d) following fuel cell testing as a methanol oxidation catalyst and reference compounds at (a and b) the Pt L_3 edge and (c and d) the Ru K edge.¹⁰² (Reproduced with permission from ref 102. Copyright 2001 American Chemical Society.)

found at approximately 1.8 Å in the Fourier transforms of the Ru K edge data for a 1:1 PtRu/C catalyst. They attributed this difference to removal of Ru from the alloy at such elevated potentials, which has been shown to occur at potentials greater than 0.7 V.¹⁰⁰ Such results may be compared with those of Nashner et al.,⁹⁵ who found that the chemisorption of oxygen on small, 1.6 nm diameter, PtRu₅/C particles was evident as Pt–O neighbors at 1.97 Å and Ru–O neighbors at 2.05 Å in the fitting of the Pt and Ru EXAFS, respectively, but did not result in a change in the metal coordination of the particles greater than the errors associated with the fitting.

The influence of the applied potential on the XAS of PtRu fuel cell catalysts is also apparent in data collected under fuel cell conditions. Viswanathan et al.³⁷ reported XANES data obtained at both the Pt L_3 and Ru K edges for a 1:1 PtRu/C catalyst prepared as a Nafion bound MEA. They found that both the Pt and Ru were metallic in both the freshly prepared MEAs and MEAs under operating conditions.

The importance of collecting such data in situ is illustrated by the work of Lin et al.¹⁰¹ and O'Grady et al.¹⁰² Lin et al. found that a commercial PtRu catalyst consisted of a mixed Pt and Ru oxide, in contrast to the catalyst prepared in their own laboratory. However, the data were collected ex situ in air. O'Grady et al. showed that even a commercial unsupported PtRu catalyst showed heavy oxidation

at both the Pt and Ru edges in the as prepared state but was metallic following treatment in a fuel cell as shown in Figure 28.

5.1.3. Adsorbates

The groups of Mukerjee^{103,104} and O'Grady^{99,105} have both reported the effects of adsorption of methanol on PtRu/C catalysts on the XANES collected at the Pt L_3 edge. Both found that at 0.0 V vs RHE the adsorption of methanol was apparent as a decrease in the broadening of the white line on the high energy side, indicating a decrease in H adsorption. In the absence of methanol, a significant increase in the white line intensity, corresponding to an increased d band vacancy per atom, is observed on increasing the potential from 0.0 to 0.5 V. In the presence of methanol, both groups found that this increase was suppressed. Swider et al.¹⁰⁵ suggested that this indicated that the methanol, or some methanol-derived fragment, donates electrons to the platinum even at such elevated potentials. Mukerjee and Urian¹⁰³ obtained data at an intermediate potential (results shown in Figure 29) and found an initial increase in the d band vacancy per atom at 0.24 V followed by a steady decline at higher potentials. They attributed the initial increase to the formation of C₁ oxide species, CO or CHO, on the surface. The decrease in d band vacancy per atom at the elevated potentials was attributed to formation of oxy-hydrox-

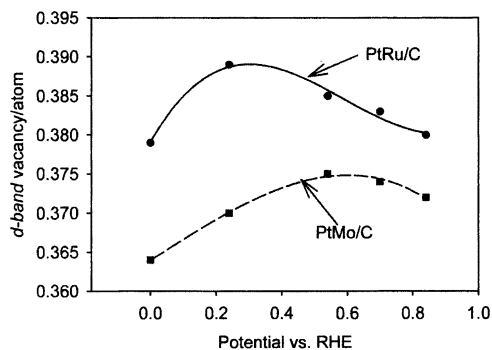


Figure 29. Pt d band vacancy per atom obtained from XANES analysis at the Pt L_3 and L_2 edges for PtRu/C (filled circles) and PtMo/C (filled squares) as a function of the applied potential in 1 mol dm^{-3} HClO_4 + 0.3 mol dm^{-3} methanol.¹⁰³ (Reproduced with permission from ref 103. Copyright 2002 Elsevier Sequoia S.A., Lausanne.)

ides of Ru on the surface of the alloy particle that displace the C_1 fragments.

5.2. Other Pt Containing Alloy Anode Catalysts

Mo alloys of Pt have also been shown to enhance the CO tolerance of PEM fuel cell catalysts.^{106–111} Two peaks are often observed in the CO stripping voltammograms for PtMo catalysts: the first at approximately 0.4 V vs RHE and the second at approximately 0.75 V. The first has been attributed to enhanced oxygen transfer from Mo oxy-hydroxide species on the surface of the catalyst particles.^{110–113} XANES at the Mo K and Pt L_3 edges has provided support for the presence of such oxy-hydroxide species. Mukerjee et al.^{103,114} have shown that the position of the Mo K edge shifts to higher energy as the potential is increased from 0.24 to 0.54 V for a 3:1 atomic ratio PtMo/C catalyst. Comparison of the edge position with those of reference compounds indicated that at 0.0 V the oxidation state of the Mo was +V, which they assigned to the hydrated oxide, $\text{MoO}(\text{OH})_2$.¹⁰³ The d band vacancy per Pt atom of PtMo/C catalysts at 0.0 V vs RHE has been shown to be greater than that observed for Pt/C.^{94,97,103,114} Increasing the potential into the double layer region, to 0.5 V, is accompanied by less of an increase in the white line intensity than observed for Pt/C. However, a significant increase is observed at 0.9 V, indicating that the Pt in PtMo catalysts is oxidized at such potentials. Thus, the second CO oxidation peak in the cyclic voltammogram is attributed to CO oxidation facilitated by the formation of oxides on the Pt sites of the catalyst.

PtMo alloys are not as effective as PtRu for methanol, or ethanol, oxidation.^{94,103} As shown in Figure 29, the d band vacancy per Pt atom for the PtMo/C catalyst continues to increase until 0.6 V vs RHE, in contrast to the behavior of PtRu/C.¹⁰³ The authors attribute this difference to the lack of removal of the C_1 fragments from the particle surface by the oxy-hydroxides of Mo. However, the difference in the electrocatalytic activity of PtRu and PtMo catalysts may be attributed to ensemble effects as well as electronic effects. The former are not probed in the white line analysis presented by Mukerjee and co-workers. In the case of methanol oxidation, en-

sembles of three active atoms have been shown to be necessary for dehydrogenation,¹¹⁵ and Mo effectively disrupts such adsorption sites while Ru does not.⁵⁸

The formation of well mixed PtMo alloys is much more difficult than that of PtRu alloys. Pt L_3 EXAFS results have been reported for PtMo/C catalysts with atomic ratios of 3:1 to 4:1 Pt/Mo.^{94,97,103} In all cases the fraction of Mo in the first coordination shell of the Pt atoms is less than that predicted from the atomic ratio. In fact, for the 4:1 catalysts examined by Neto et al.,⁹⁴ the data did not support the inclusion of any Mo neighbors. Combined with the average +V oxidation state of the Mo at 0.0 V reported by Mukerjee,¹⁰³ these results support the view that the PtMo/C catalysts investigated thus far may be described as Pt particles modified by a small amount of Mo and a separate Mo oxide phase. Crabb et al.¹¹⁶ have developed a method that ensures that all of the Mo in the catalyst is associated with the Pt. Using a controlled surface reaction, in which an organometallic precursor of the Mo is reacted with the reduced Pt surface, they prepared Pt/C catalysts modified by submonolayer coverages of Mo. EXAFS collected at the Mo K edge verified that the Mo was in contact with the Pt but was present as an oxide or oxy-hydroxide species in the as prepared catalyst, before application of an applied potential, and at 0.65 V vs RHE. Upon electrochemical reduction at 0.05 V, the number of Pt neighbors in the first coordination shell increased from 0.8 to 4.5, indicating that the Mo was then incorporated into the surface of the metal particle. This catalyst also exhibited improved CO tolerance at low potentials compared to the case of the unmodified Pt/C catalyst, providing added evidence of the role of the oxy-hydroxides of Mo in the enhancement mechanism.

Mukerjee and McBreen have also investigated PtSn/C alloy catalysts and Pt/C catalysts modified by upd layers of Sn,^{117,118} both of which had previously been shown to have enhanced catalytic activity for methanol oxidation.^{115,119,120} They found that the alloy consisted of the Pt_3Sn fcc phase with an increased Pt–Pt bond distance. In contrast to the cases of PtRu and PtMo, the formation of the Sn alloy was accompanied by a decrease in the d band vacancy per Pt atom. Pt XANES results for the upd of Sn on Pt/C showed minimal effects on the d band vacancies of the Pt atoms, and analysis of the EXAFS confirmed that the Pt–Pt distance remained unchanged. EXAFS at the Sn edge for both the upd modified Pt and the $\text{Pt}_3\text{Sn}/\text{C}$ alloy showed Sn–O interactions at all potentials in the range 0.0–0.54 V vs RHE. From these results the authors drew the conclusions that the Sn provides oxygen species to the Pt that enhance methanol oxidation, and that the improved performance of the upd of Sn on Pt/C compared to the alloy was related to the decreased number of sites for dissociative adsorption of methanol on the surface of the Pt_3Sn alloy.

5.3. Pt Containing Alloy Cathode Catalysts

The kinetics of the four electron oxygen reduction reaction at Pt are limited by the very low exchange

current density under the acidic conditions present in both phosphoric acid and low temperature/PEM fuel cells.^{121,122} The electrocatalytic activity of Pt catalyst particles for the oxygen reduction reaction has been shown to improve by alloying with first row transition elements in both phosphoric acid fuel cells^{123–125} and low temperature PEM fuel cells.¹²⁶ Mukerjee et al.^{34,127,128} have shown that XAS studies are uniquely suited to quantifying both the structural and electronic effects of alloying which result from this enhancement.

Mukerjee et al.³⁴ investigated the electrocatalysis of the oxygen reduction reaction at five binary Pt alloys, PtCr/C, PtMn/C, PtFe/C, PtCo/C, and PtNi/C. The kinetics of the oxygen reduction reaction were assessed by measuring the current at 0.9 V vs RHE in a single cell PEM fuel cell at 95 °C and 5 atm pressure of humidified O₂. Enhanced electrocatalysis compared to that of Pt/C was found for all of the alloys investigated, with the best performance reported for the PtCr/C catalyst. XAS data were collected at the Pt L₃ and L₂ edges as well as the K edge of the secondary element for each of the catalysts as a function of the applied potential in 1 mol dm⁻³ HClO₄. To avoid complications in the analysis of the XAS data, the catalysts were subjected to leaching in either 2 mol dm⁻³ KOH, for the PtCr/C, or 1 mol dm⁻³ HClO₄, for all the others, to remove any residual oxides or unalloyed first row transition elements. The catalysts used in the fuel cell measurements were not subjected to such pretreatment.

XANES analysis at the Pt L edges and the K edges of the secondary elements was used to determine the d band occupancy of the Pt atoms in the catalysts and to provide evidence of any redox behavior of the secondary element, respectively. The EXAFS obtained at the Pt L₃ edge verified the presence of the alloy phase as well as a measure of the Pt–Pt bond distance. The results indicated that the electrocatalysis of the oxygen reduction reaction is related to the vacancies of the d band, the Pt–Pt bond distance, and suppression of oxide formation on the surface of the particles. No evidence of redox behavior of the secondary element was found; that is, the position of the absorption edge was not found to be potential dependent. A plot of the electrocatalytic activity versus the electronic (Pt d band vacancies per atom) and geometric (Pt–Pt bond distance) parameters was found to exhibit volcano type behavior, as shown in Figure 30. It should be noted that the order of the d-orbital vacancy points (from left to right, Pt/C, PtMn/C, PtCr/C, PtFe/C, PtCo/C, and PtNi/C) is opposite that for the Pt–Pt bond distance. In both cases the PtCr/C catalyst is found near the top of the volcano curves, indicating that it has the best combination of Pt d band vacancies and contraction of the Pt–Pt bond distance. Such an interplay between d band vacancies, Pt–Pt bond distance, and oxygen reduction activity was also found in studies of the effects of the particle size of binary Pt alloys by Mukerjee et al.¹²⁸ and Min et al.¹²⁹

In a later study of the same series of binary catalysts, Mukerjee and McBreen¹²⁷ showed that the restructuring accompanying the desorption of ad-

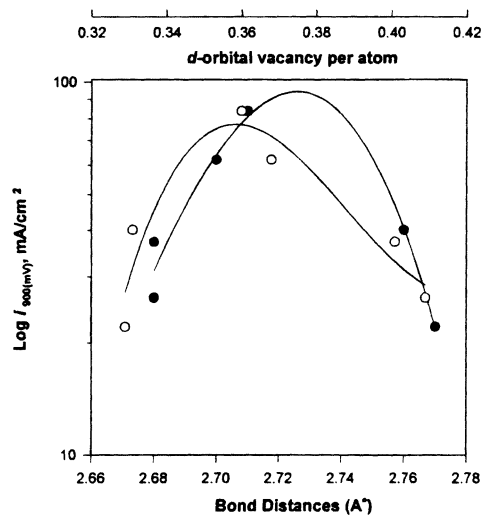


Figure 30. Correlation of the oxygen reduction performance ($\log j_{900 \text{ mV}}$) of Pt and Pt alloy electrocatalysts in a PEM fuel cell with Pt–Pt bond distance (filled circles) and the d band vacancy per atom (open circles) obtained from in situ XAS at the Pt L₃ and L₂ edges.³⁴ (Reproduced with permission from ref 34. Copyright 1995 The Electrochemical Society, Inc.)

sorbed hydrogen previously reported for Pt/C particles⁶⁰ did not occur for these alloys. They also reported that the surfaces of alloy catalysts consist of a Pt skin on the basis of the similarity of the electrochemically determined hydrogen coverages to that of Pt/C. However, EXAFS analysis was not reported for the K edge of the secondary element to support this statement.

Ternary and more complex alloys are now the subjects of investigations that seek further improvements in oxygen reduction activity.^{126,130–136} Structural characterization of such systems using EXAFS methods becomes increasingly complex. XAS data should be collected at absorption edges corresponding to each element in the alloy, but this is not always possible, for example, when the absorption edges of the elements overlap. Kim et al.^{137,138} have reported an XAS study of the ternary alloy, PtCuFe/C. The XAS data were collected at the Pt L₃ edge for powders of PtCuFe/C catalysts of varying Pt content, and Pt₂CuFe and Pt₆CuFe subjected to heat treatments between 500 and 1100 °C. The analysis of the EXAFS data highlights the difficulty in separating the contributions from neighbors that have similar atomic number and, therefore, similar backscattering amplitudes and phase shifts. The contributions of the Cu and Fe could not be reliably separated, and although they were fitted independently, the distances and coordination numbers for the two contributions were found to be the same within the error limit. The ratios of the coordination numbers for the Pt and non-Pt neighbors were in good agreement with their bulk contents, indicating that well ordered alloys were formed. As in the case of the binary alloys, PtCu/C and PtFe/C, a reduced Pt–Pt bond distance, as compared to that for Pt/C, was found. Enhanced mass activities for oxygen reduction were found for the ternary alloys and were attributed to the formation of the ordered alloy phases.

6. Non-Pt Catalysts

Most of the catalysts employed in PEM and direct methanol fuel cells, DMFCs, are based on Pt, as discussed above. However, when used as cathode catalysts in DMFCs, Pt containing catalysts can become poisoned by methanol that crosses over from the anode. Thus, considerable effort has been invested in the search for both methanol resistant membranes and cathode catalysts that are tolerant to methanol. Two classes of catalysts have been shown to exhibit oxygen reduction catalysis and methanol resistance, ruthenium chalcogen based catalysts^{126,139–143} and metal macrocycle complexes, such as porphyrins or phthalocyanines.^{144,145}

EXAFS has been used by Alonso-Vante and co-workers^{146–149} to characterize a series of Ru chalcogenide compounds in situ for catalyst particles deposited onto a conducting SnO₂:F glass support in 0.5 mol dm⁻³ H₂SO₄. The data were collected in reflectance mode with an incident angle of ≤ 1.5 mrad at the Ru K edge. The signal-to-noise ratio of the data collected was very poor, as shown in Figure 31, because it was limited by the thickness of the sample and the collection method. Better results may have been obtained if the data had been collected as fluorescence. Nevertheless, the authors have shown that the catalysts consist of small Ru particles that are stabilized by the presence of the chalcogen, S, Se, or Te, as evidenced by the presence of both chalcogen

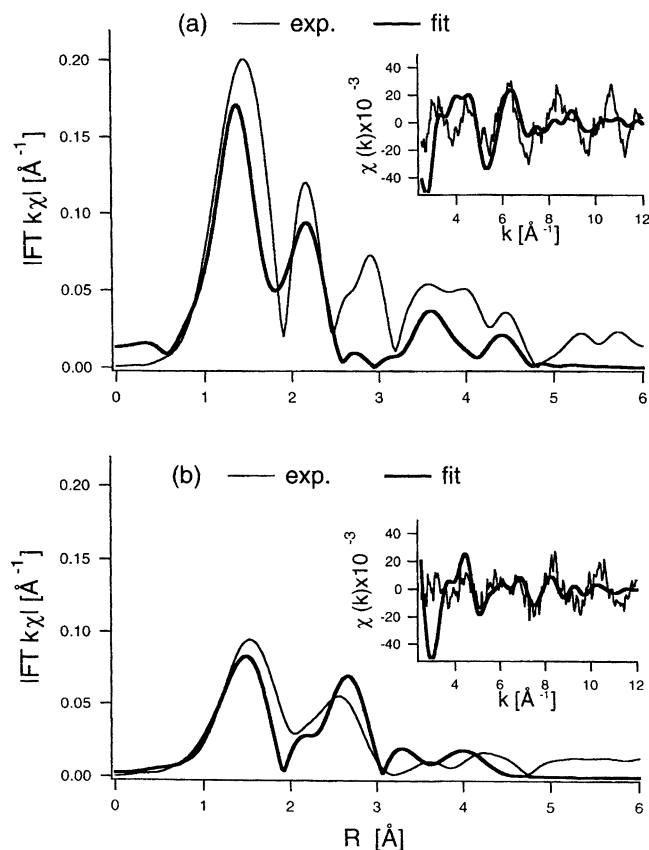


Figure 31. Ru K EXAFS data (insets) and corresponding Fourier transforms for Ru_xSe_y particles on a SnO₂:F support in (a) nitrogen and (b) oxygen saturated 0.5 mol dm⁻³ H₂SO₄: experimental data (thin lines) and fits (thick lines).¹⁴⁹ (Reproduced with permission from ref 149. Copyright 2000 Elsevier Sequoia S.A., Lausanne.)

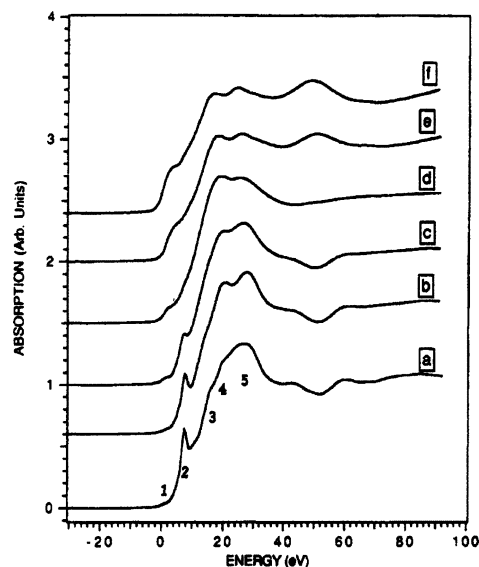


Figure 32. Co K edge XANES for (a) cobalt phthalocyanine (PcCo), (b–e) PcCo on Vulcan XC-72 [(b) untreated sample; (c–e) sample heated to (c) 700 °C, (d) 800 °C, and (e) 1000 °C], and (f) Co metal.¹⁵⁵ (Reproduced with permission from ref 155. Copyright 1992 American Chemical Society.)

and Ru neighbors in the first coordination shell. The local structure surrounding Ru in these catalysts was found to depend on the presence of oxygen in the solution, as also shown in Figure 31, but not on the applied potential. However, the materials are likely to consist of a mixture of phases, and therefore, as EXAFS results reflect the average coordination, the results cannot provide a detailed structural model of these catalysts.

The nature of the catalytic center in oxygen reduction catalysts prepared by the heat treatment of N₄-metal chelates on carbon supports has caused much debate, in particular whether the N₄-metal center is retained in the catalyst. In two early EXAFS studies Joyner et al.¹⁵⁰ and van Wingerden et al.¹⁵¹ showed that the N₄-metal center was retained in carbon supported Co-porphyrin catalysts exposed to temperatures as high as 850 °C. Martins Alves et al. later showed that this center was destroyed at higher temperatures, leaving Co particles on the carbon support. The XANES region for Co phthalocyanine, PcCo, on Vulcan XC-72 subjected to heating to various temperatures under an argon atmosphere is shown in Figure 32. The XANES of the pure PcCo reflects the square planar D_{4h} symmetry of the Co, and the peak labeled 2 provides a fingerprint of the Co–N₄ structure. For temperatures above 700 °C this peak is no longer observed, indicating a loss of the square planar configuration, and the XANES is very similar to that obtained for Co metal. These observations are confirmed by the Fourier transforms of the EXAFS as shown in Figure 33. The Fourier transform of the PcCo exhibits a peak at 1.6 Å for the Co–N distance. As the annealing temperature is increased, the amplitude of this peak decreases and a new peak grows in at 2.2 Å, corresponding to the Co–Co bond, indicating the formation of Co particles. The best oxygen reduction activity was obtained with the catalysts prepared by annealing to 850 °C,

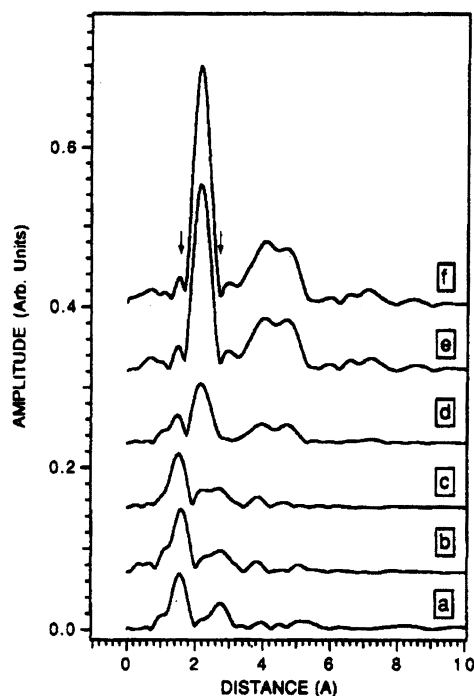


Figure 33. Fourier transforms of the Cu K EXAFS data for the samples described in Figure 32.¹⁵⁵ (Reproduced with permission from ref 155. Copyright 1992 American Chemical Society.)

corresponding to loss of the Co–N₄ center with the smallest Co particles.

The presence of Fe–N₄ was reported by Choi et al. for iron phthalocyanine on carbon,¹⁵² with the formation of an Fe₂O₃-like structure above 900 °C, and by Bron et al. for iron phenanthroline on carbon.¹⁵³ However, it is very difficult to give any weight to the conclusions of Bron et al. based on their EXAFS results, as figures depicting neither the data nor the fit are shown nor is a statistical measure of the goodness of fit reported. The results reported by Choi et al.¹⁵² indicate that the loss of electrocatalytic activity at higher annealing temperatures is more likely to be related to the formation of the inactive Fe₂O₃ phase rather than the loss of the Fe–N₄ center.

7. Conclusion

XAS has been successfully employed in the characterization of a number of catalysts used in low temperature fuel cells. Analysis of the XANES region has enabled determination of the oxidation state of metal atoms in the catalyst or, in the case of Pt, the d band vacancy per atom, while analysis of the EXAFS has proved to be a valuable structural tool. However, the principal advantage of XAS is that it can be used in situ, in a flooded half-cell or true fuel cell environment. While the number of publications has been limited thus far, the increased availability of synchrotron radiation sources, improvements in beam lines brought about by the development of third generation sources, and the development of more readily used analysis software should increase the accessibility of the method. It is hoped that this review will enable the nonexpert to understand both the power and limitations of XAS in characterizing fuel cell electrocatalysts.

8. References

- Ankudinov, A. L.; Ravel, B.; Rehr, J. J.; Conradson, S. D. *Phys. Rev. B* **1998**, *58*, 7565.
- Ankudinov, A. L.; Rehr, J. J.; Low, J. J.; Bare, S. R. *Top. Catal.* **2002**, *18*, 3.
- Bazin, D.; Sayers, D.; Rehr, J. J.; Mottet, C. *J. Phys. Chem. B* **1997**, *101*, 5332.
- Ankudinov, A. L.; Rehr, J. J.; Low, J. J.; Bare, S. R. *J. Chem. Phys.* **2002**, *116*, 1911.
- Bazin, D.; Rehr, J. J. *J. Phys. Chem. B* **2003**, *107*, 12398.
- Cauchois, Y.; Mott, N. F. *Philos. Mag.* **1949**, *40*, 1260.
- Mansour, A. N.; Cook, J. W.; Sayers, D. E. *J. Phys. Chem.* **1984**, *88*, 2330.
- Brown, M.; Peierls, R. E.; Stern, D. E. *Phys. Rev. B* **1977**, *15*, 738.
- Koningsberger, D. C.; Prins, R. *X-ray Absorption*; John Wiley and Sons: New York, 1988.
- Teo, B. K. *EXAFS: Basic principles and data analysis*; Springer-Verlag: Berlin, 1986.
- Rehr, J. J.; Albers, R. C.; Sabinsky, S. I. *Phys. Rev. Lett.* **1992**, *69*, 3397.
- Rehr, J. J.; Albers, R. C. *Phys. Rev. B* **1990**, *41*, 8139.
- Zabinsky, S. I.; Rehr, J. J.; Ankudinov, A.; Albers, R. C.; Eller, M. J. *Phys. Rev. B* **1996**, *52*.
- <http://ixs.csrii.iit.edu/IXS/>.
- Ankudinov, A. L.; Conradson, S. D.; de Leon, J. M.; Rehr, J. J. *Phys. Rev. B* **1998**, *57*, 7518.
- Gurman, S. J.; Binsted, N.; Ross, I. *J. Phys. C* **1984**, *17*, 143.
- Duivendoorn, F. B. M.; Koningsberger, D. C.; Uh, Y. S.; Gates, B. C. *J. Am. Chem. Soc.* **1986**, *108*, 6254.
- Error reporting recommendations: a report of the standards and criteria committee; IXS Standards and Criteria Committee: 2000.
- Koningsberger, D. C.; Mojet, B. L.; van Dorssen, G. E.; Ramaker, D. E. *Top. Catal.* **2000**, *10*, 143.
- Li, G. G.; Bridges, F.; Booth, C. H. *Phys. Rev. B* **1995**, *52*, 6332.
- Stern, E. A. *Phys. Rev. B* **1993**, *48*, 9825.
- Young, N. A.; Dent, A. J. *J. Synchrotron Radiat.* **1999**, *6*, 799.
- Koningsberger, D. C. *Jpn. J. Appl. Phys., Part 1: Regul. Pap., Short Notes Rev. Pap.* **1993**, *32*, 877.
- McMaster, W. H.; Kerr Del Grande, N.; Mallett, J. H.; Hubbell, J. H. *Compilation of X-ray Cross Sections*; U.S. Department of Commerce: 1969; Vol. UCRL-50174, Section II, Revision I.
- Mathew, R. J.; Russell, A. E. *Top. Catal.* **2000**, *10*, 231.
- Allen, P. G.; Conradson, S. D.; Pennerhahn, J. E. *J. Appl. Crystallogr.* **1993**, *26*, 172.
- Dent, A.; Evans, J.; Newton, M.; Corker, J.; Russell, A.; Abdul Rahman, A. B.; Fiddy, S.; Mathew, R.; Farrow, R.; Salvini, G.; Atkinson, P. *J. Synchrotron Radiat.* **1999**, *6*, 381.
- Sharpe, L. R.; Heineman, W. R.; Elder, R. C. *Chem. Rev.* **1990**, *90*, 705.
- O'Grady, W. E.; Koningsberger, D. C. *Ext. Abstr. Electrochem. Soc.* **1988**, *88-1*, 736.
- Lampitt, R. A.; Carrette, L. P. L.; Hogarth, M. P.; Russell, A. E. *J. Electroanal. Chem.* **1999**, *460*, 80.
- McBreen, J.; O'Grady, W. E.; Pandya, K. I.; Hoffman, R. W.; Sayers, D. E. *Langmuir* **1987**, *3*, 428.
- Herron, M. E.; Doyle, S. E.; Pizzini, S.; Roberts, K. J.; Robinson, J.; Hards, G.; Walsh, F. C. *J. Electroanal. Chem.* **1992**, *324*, 243.
- Maniguet, S.; Mathew, R. J.; Russell, A. E. *J. Phys. Chem. B* **2000**, *104*, 1998.
- Mukerjee, S.; Srinivasan, S.; Soriaga, M. P.; McBreen, J. *J. Electrochem. Soc.* **1995**, *142*, 1409.
- Adzic, R. R.; Wang, J. X.; Ocko, B. M.; McBreen, J. EXAFS, XANES, SXS. In *Handbook of Fuel Cells—Fundamentals, Technology and Applications*; Vielstich, W., Gasteiger, H. A., Lamm, A., Eds.; John Wiley and Sons, Ltd.: New York, 2003; Vol. 2; p 277.
- Roth, C.; Martz, N.; Buhrmester, T.; Scherer, J.; Fuess, H. *Phys. Chem. Chem. Phys.* **2002**, *4*, 3555.
- Viswanathan, R.; Hou, G. Y.; Liu, R. X.; Bare, S. R.; Modica, F.; Mickelson, G.; Segre, C. U.; Leyarovska, N.; Smotkin, E. S. *J. Phys. Chem. B* **2002**, *106*, 3458.
- O'Grady, W. E.; Heald, S. M.; Sayers, D. E.; Budnick, J. I. *Ext. Abstr. Electrochem. Soc.* **1983**, *83-1*, 1071.
- Yoshitake, H.; Yamazaki, O.; Ota, K. *J. Electrochem. Soc.* **1994**, *141*, 2516.
- Yoshitake, H.; Mochizuki, T.; Yamazaki, O.; Ota, K. *J. Electroanal. Chem.* **1993**, *361*, 229.
- Allen, P. G.; Conradson, S. D.; Wilson, M. S.; Gottesfeld, S.; Raistrick, I. D.; Valerio, J.; Lovato, M. *Electrochim. Acta* **1994**, *39*, 2415.
- Yoshitake, H.; Yamazaki, O.; Ota, K. *J. Electroanal. Chem.* **1994**, *371*, 287.
- Allen, P. G.; Conradson, S. D.; Wilson, M. S.; Gottesfeld, S.; Raistrick, I. D.; Valerio, J.; Lovato, M. *J. Electroanal. Chem.* **1995**, *384*, 99.

- (44) Chang, J. R.; Lee, J. F.; Lin, S. D.; Lin, A. S. *J. Phys. Chem.* **1995**, *99*, 14798.
- (45) McBreen, J.; Mukerjee, S. *Ext. Abstr. Electrochem. Soc.* **1996**, *96-2*, 125.
- (46) Mukerjee, S.; McBreen, J. *J. Electroanal. Chem.* **1998**, *448*, 163.
- (47) O'Grady, W. E.; Ramaker, D. E. *Electrochim. Acta* **1998**, *44*, 1283.
- (48) O'Grady, W. E.; Ramaker, D. E. *Ext. Abstr. Electrochem. Soc.* **1999**, *99-1*, 1034.
- (49) O'Grady, W. E.; Ramaker, D. E. *J. Synchrotron Radiat.* **1999**, *6*, 599.
- (50) Ramaker, D. E.; O'Grady, W. E. *Ext. Abstr. Electrochem. Soc.* **2001**, *2001-1*, 1038.
- (51) Teliska, M.; O'Grady, W. E.; Ramaker, D. E. *Ext. Abstr. Electrochem. Soc.* **2002**, *2002-1*, 1330.
- (52) O'Grady, W. E.; Hagans, P. L. *Ext. Abstr. Electrochem. Soc.* **2003**, *2003-1*, 2851.
- (53) Mansour, A. N.; Sayers, D. E.; Cook, J. W.; Short, D. R.; Shannon, R. D.; Katzer, J. R. *J. Phys. Chem.* **1984**, *88*, 1778.
- (54) Mansour, A. N.; Cook, J. W.; Sayers, D. E.; Emrich, R. J.; Katzer, J. R. *J. Catal.* **1984**, *89*, 464.
- (55) Samant, M. G.; Boudart, M. *J. Phys. Chem.* **1991**, *95*, 4070.
- (56) Kinoshita, K. *Electrochemical Oxygen Technology*; Wiley: New York, 1992.
- (57) Markovic, N.; Gasteiger, H.; Ross, P. N. *J. Electrochem. Soc.* **1997**, *144*, 1591.
- (58) Markovic, N. M.; Ross, P. N. *Surf. Sci. Rep.* **2002**, *45*, 121.
- (59) Benfield, R. E. *J. Chem. Soc., Faraday Trans.* **1992**, *88*, 1107.
- (60) McBreen, J.; Mukerjee, S. *J. Electrochem. Soc.* **1995**, *142*, 3399.
- (61) Doyle, S. E.; Roberts, K. J.; Herron, M. E.; Robinson, J.; Walsh, F. C. In *X-ray Absorption Fine Structure*; Hasnain, S. S., Ed.; Ellis Horwood: Chichester, U.K., 1991; p 279.
- (62) Dent, A. J. *Top. Catal.* **2002**, *18*, 27.
- (63) Angerstein-Kozłowska, H.; Conway, B. E. *J. Electroanal. Chem.* **1979**, *95*, 26.
- (64) Angerstein-Kozłowska, H.; Conway, B. E.; Sharp, W. B. A. *J. Electroanal. Chem.* **1973**, *43*, 9.
- (65) Conway, B. E.; Barnett, B.; Angerstein-Kozłowska, H.; Tilak, B. V. *J. Chem. Phys.* **1990**, *93*, 8361.
- (66) O'Grady, W. E.; Qian, X.; Ramaker, D. E. *J. Phys. Chem. B* **1997**, *101*, 5624.
- (67) Holland, B. W.; Pendry, J. B.; Pettifer, R. F.; Bordas, J. J. *J. Phys. C* **1978**, *11*, 633.
- (68) Rehr, J. J.; Booth, C. H.; Bridges, F.; Zabinsky, S. I. *Phys. Rev. B* **1994**, *49*, 12347.
- (69) Ankudinov, A. L.; Rehr, J. J. *Phys. Rev. B* **1997**, *56*, R1712.
- (70) Ankudinov, A. L.; Rehr, J. J. *J. Phys. IV* **1997**, *7*, 121.
- (71) Filipponi, A.; DiCicco, A. *Phys. Rev. B* **1996**, *53*, 9466.
- (72) McBreen, J. *J. Electroanal. Chem.* **1993**, *357*, 373.
- (73) McBreen, J.; Ogrady, W. E.; Tourillon, G.; Dartyge, E.; Fontaine, A. *J. Electroanal. Chem.* **1991**, *307*, 229.
- (74) McBreen, J.; Sansone, M. *J. Electroanal. Chem.* **1994**, *373*, 227.
- (75) Yoshitake, H.; Yamazaki, O.; Ota, K. I. *J. Electroanal. Chem.* **1995**, *387*, 135.
- (76) Lucas, C. A.; Markovic, N. M.; Ross, P. N. *Phys. Rev. B* **1997**, *56*, 3651.
- (77) Toney, M. F.; Howard, J. N.; Richer, J.; Borges, G. L.; Gordon, J. G.; Melroy, O. R. *Phys. Rev. Lett.* **1995**, *75*, 4472.
- (78) Shi, Z.; Lipkowski, J. *J. Electroanal. Chem.* **1994**, *364*, 289.
- (79) Alexeev, O. S.; Graham, G. W.; Shelef, M.; Adams, R. D.; Gates, B. C. *J. Phys. Chem. B* **2002**, *106*, 4697.
- (80) Mojte, B. L.; Ramaker, D. E.; Miller, J. T.; Koningsberger, D. C. *Catal. Lett.* **1999**, *62*, 15.
- (81) Campbell, C. T. *Annu. Rev. Phys. Chem.* **1990**, *41*, 775.
- (82) Gasteiger, H. A.; Markovic, N. M.; Ross, P. N. *J. Phys. Chem.* **1995**, *99*, 16757.
- (83) Gasteiger, H. A.; Markovic, N. M.; Ross, P. N. *J. Phys. Chem.* **1995**, *99*, 8290.
- (84) Watanabe, M.; Motoo, S. *J. Electroanal. Chem.* **1975**, *60*, 275.
- (85) Watanabe, M.; Uchida, M.; Motoo, S. *J. Electroanal. Chem.* **1987**, *229*, 395.
- (86) Cameron, D. S.; Hards, G. A.; Thompsett, D. Workshop on direct methanol-air fuel cells, 1992.
- (87) Maniguet, S. EXAFS studies of carbon supported fuel cells electrocatalysts. Ph.D. Thesis, University of Southampton, 2002.
- (88) Pandya, K. I.; Anderson, E. B.; Sayers, D. E.; Ogrady, W. E. *J. Phys. IV* **1997**, *7*, 955.
- (89) Binsted, N. *EXCURVE98*; Daresbury Laboratory: Warrington, U.K., 1998.
- (90) Camara, G. A.; Giz, M. J.; Paganin, V. A.; Ticianelli, E. A. *J. Electroanal. Chem.* **2002**, *537*, 21.
- (91) Meitzner, G.; Via, G. H.; Lytle, F. W.; Sinfelt, J. H. *Physica B* **1989**, *158*, 138.
- (92) Page, T.; Johnson, R.; Hormes, J.; Noding, S.; Rambabu, B. *J. Electroanal. Chem.* **2000**, *485*, 34.
- (93) Ertel, T. S.; Bertagnoli, H.; Huckmann, S.; Kolb, U.; Peter, D. *Appl. Spectrosc.* **1992**, *46*, 690.
- (94) Neto, A. O.; Giz, M. J.; Perez, J.; Ticianelli, E. A.; Gonzalez, E. R. *J. Electrochem. Soc.* **2002**, *149*, A272.
- (95) Nashner, M. S.; Somerville, D. M.; Lane, P. D.; Adler, D. L.; Shapley, J. R.; Nuzzo, R. G. *J. Am. Chem. Soc.* **1996**, *118*, 12964.
- (96) Nashner, M. S.; Frenkel, A. I.; Somerville, D.; Hills, C. W.; Shapley, J. R.; Nuzzo, R. G. *J. Am. Chem. Soc.* **1998**, *120*, 8093.
- (97) Russell, A. E.; Maniguet, S.; Mathew, R. J.; Yao, J.; Roberts, M. A.; Thompsett, D. *J. Power Sources* **2001**, *96*, 226.
- (98) Kabbabi, A.; Durand, R.; Faure, R. *Ext. Abstr. Electrochem. Soc.* **1995**, *95-1*, 750.
- (99) O'Grady, W. E.; Swider, K. E.; Pandya, K. I.; Kowalak, A. D. *Ext. Abstr. Electrochem. Soc.* **1995**, *95-1*, 744.
- (100) Gasteiger, H. A.; Markovic, N.; Ross, P. N.; Cairns, E. J. *J. Phys. Chem.* **1994**, *98*, 617.
- (101) Lin, S. D.; Hsiao, T. C.; Chang, J. R.; Lin, A. S. *J. Phys. Chem. B* **1999**, *103*, 97.
- (102) O'Grady, W. E.; Hagans, P. L.; Pandya, K. I.; Maricle, D. L. *Langmuir* **2001**, *17*, 3047.
- (103) Mukerjee, S.; Urian, R. C. *Electrochim. Acta* **2002**, *47*, 3219.
- (104) Mukerjee, S.; McBreen, J. *Ext. Abstr. Electrochem. Soc.* **1996**, *96-1*, 1130.
- (105) Swider, K. E.; Pandya, K. I.; Kowalak, A. D.; Hagans, P. L.; O'Grady, W. E. *Ext. Abstr. Electrochem. Soc.* **1995**, *95-1*, 742.
- (106) Grgur, B. N.; Markovic, N. M.; Ross, P. N. *J. Serb. Chem. Soc.* **2003**, *68*, 191.
- (107) Ball, S.; Hodgkinson, A.; Hoogers, G.; Maniguet, S.; Thompsett, D.; Wong, B. *Electrochem. Solid State Lett.* **2002**, *5*, A31.
- (108) Grgur, B. N.; Markovic, N. M.; Ross, P. N. *J. Electrochem. Soc.* **1999**, *146*, 1613.
- (109) Mukerjee, S.; Lee, S. J.; Ticianelli, E. A.; McBreen, J.; Grgur, B. N.; Markovic, N. M.; Ross, P. N.; Gialombardo, J. R.; De Castro, E. S. *Electrochem. Solid State Lett.* **1999**, *2*, 12.
- (110) Grgur, B. N.; Markovic, N. M.; Ross, P. N. *J. Phys. Chem. B* **1998**, *102*, 2494.
- (111) Grgur, B. N.; Zhuang, G.; Markovic, N. M.; Ross, P. N. *J. Phys. Chem. B* **1997**, *101*, 3910.
- (112) Grgur, B. N.; Markovic, N. M.; Ross, P. N. *Proton Conducting Membrane Fuel Cells*; 1999.
- (113) Zhang, H. Q.; Wang, Y.; Fachini, E. R.; Cabrera, C. R. *Electrochem. Solid State Lett.* **1999**, *2*, 437.
- (114) Mukerjee, S.; Lee, S. J.; Ticianelli, E. A.; McBreen, J. *Ext. Abstr. Electrochem. Soc.* **1998**, *98-2*, 1087.
- (115) Wang, K.; Gasteiger, H. A.; Markovic, N. M.; Ross, P. N. *Electrochim. Acta* **1996**, *41*, 2587.
- (116) Crabb, E. M.; Ravikumar, M. K.; Qian, Y.; Russell, A. E.; Maniguet, S.; Yao, J.; Thompsett, D.; Hurford, M.; Ball, S. C. *Electrochem. Solid State Lett.* **2002**, *5*, A5.
- (117) Mukerjee, S.; McBreen, J. *J. Electrochem. Soc.* **1999**, *146*, 600.
- (118) Mukerjee, S.; McBreen, J. *Ext. Abstr. Electrochem. Soc.* **1996**, *96-2*, 127.
- (119) Campbell, S. A.; Parsons, R. *J. Chem. Soc., Faraday Trans.* **1992**, *88*, 833.
- (120) Haner, A. N.; Ross, P. N. *J. Phys. Chem.* **1991**, *95*, 3740.
- (121) Srinivasan, S. *J. Electrochem. Soc.* **1989**, *136*, C41.
- (122) Appleby, A. J.; Foulkes, F. R. *Fuel Cell Handbook*; van Norstrand Reinhold: New York, 1989.
- (123) Jalan, V. M. U.S. Patent, 4,202,934, 1980.
- (124) Landsman, D. A.; Laczak, F. J. U.S. Patent, 4,36,944, 1982.
- (125) Mukerjee, S. *J. Appl. Electrochem.* **1990**, *20*, 537.
- (126) Mukerjee, S.; Srinivasan, S. *J. Electroanal. Chem.* **1993**, *357*, 201.
- (127) Mukerjee, S.; McBreen, J. *J. Electrochem. Soc.* **1996**, *143*, 2285.
- (128) Mukerjee, S.; Srinivasan, S.; Soriaga, M. P.; McBreen, J. *J. Phys. Chem.* **1995**, *99*, 4577.
- (129) Min, M. K.; Cho, J. H.; Cho, K. W.; Kim, H. *Electrochim. Acta* **2000**, *45*, 4211.
- (130) Smotkin, E. S.; Diaz-Morales, R. R. *Annu. Rev. Mater. Res.* **2003**, *33*, 557.
- (131) Paulus, U. A.; Wokaun, A.; Scherer, G. G.; Schmidt, T. J.; Stamenkovic, V.; Markovic, N. M.; Ross, P. N. *Electrochim. Acta* **2002**, *47*, 3787.
- (132) Chen, G. Y.; Delafuente, D. A.; Sarangapani, S.; Mallouk, T. E. *Catal. Today* **2001**, *67*, 341.
- (133) Shukla, A. K.; Neergat, M.; Bera, P.; Jayaram, V.; Hegde, M. S. *J. Electroanal. Chem.* **2001**, *504*, 111.
- (134) Neergat, M.; Shukla, A. K.; Gandhi, K. S. *J. Appl. Electrochem.* **2001**, *31*, 373.
- (135) Li, Y. J.; Chang, C. C.; Wen, T. C. *J. Appl. Electrochem.* **1997**, *27*, 227.
- (136) Tamizhmani, G.; Capuano, G. A. *J. Electrochem. Soc.* **1994**, *141*, 968.
- (137) Cho, J. H.; Roh, W. J.; Kim, D. K.; Yoon, J. B.; Choy, J. H.; Kim, H. S. *J. Chem. Soc., Faraday Trans.* **1998**, *94*, 2835.
- (138) Kim, D. K.; Choy, J. H.; Han, K. S.; Hwang, S. J.; Roh, W.; Kim, H. *J. Phys. IV* **1997**, *7*, 953.
- (139) Hilgendorff, M.; Diesner, K.; Schulenburg, H.; Bogdanoff, P.; Bron, M.; Fiechter, S. *J. New Mater. Electrochem. Syst.* **2002**, *5*, 71.
- (140) Tributsch, H.; Bron, M.; Hilgendorff, M.; Schulenburg, H.; Dorbandt, I.; Eyert, V.; Bogdanoff, P.; Fiechter, S. *J. Appl. Electrochem.* **2001**, *31*, 739.

- (141) Bron, M.; Bogdanoff, P.; Fiechter, S.; Dorbandt, I.; Hilgendorff, M.; Schulenburg, H.; Tributsch, H. *J. Electroanal. Chem.* **2001**, *500*, 510.
- (142) Reeve, R. W.; Christensen, P. A.; Dickinson, A. J.; Hamnett, A.; Scott, K. *Electrochim. Acta* **2000**, *45*, 4237.
- (143) Reeve, R. W.; Christensen, P. A.; Hamnett, A.; Haydock, S. A.; Roy, S. C. *J. Electrochem. Soc.* **1998**, *145*, 3463.
- (144) Jasinski, R. *J. Electrochem. Soc.* **1965**, *112*, 526.
- (145) Jahnke, H.; Schönborn, M.; Zimmermann, G. *Top. Curr. Chem.* **1976**, *61*, 133.
- (146) Alonso-Vante, N.; Malakhov, I. V.; Nikitenko, S. G.; Savinova, E. R.; Kochubey, D. I. *Electrochim. Acta* **2002**, *47*, 3807.
- (147) Malakhov, I. V.; Nikitenko, S. G.; Savinova, E. R.; Kochubey, D. I.; Alonso-Vante, N. *J. Phys. Chem. B* **2002**, *106*, 1670.
- (148) Malakhov, I. V.; Nikitenko, S. G.; Savinova, E. R.; Kochubey, D. I.; Alonso-Vante, N. *Nucl. Instrum. Methods Phys. Res., Sect. A: Accel., Spectrom., Dect., Assoc. Equip.* **2000**, *448*, 323.
- (149) Alonso-Vante, N.; Borthen, P.; Fieber-Erdmann, M.; Strehblow, H. H.; Holub-Krappe, E. *Electrochim. Acta* **2000**, *45*, 4227.
- (150) Joyner, R. W.; Vanveen, J. A. R.; Sachtler, W. M. H. *J. Chem. Soc., Faraday Trans. 1* **1982**, *78*, 1021.
- (151) van Wingerden, B.; Vanveen, J. A. R.; Mensch, C. T. J. *J. Chem. Soc., Faraday Trans. 1* **1988**, *84*, 65.
- (152) Choi, H. J.; Kwag, G.; Kim, S. *J. Electroanal. Chem.* **2001**, *508*, 105.
- (153) Bron, M.; Radnik, J.; Fieber-Erdmann, M.; Bogdanoff, P.; Fiechter, S. *J. Electroanal. Chem.* **2002**, *535*, 113.
- (154) Mojet, B. L. Metal-support interactions: a step closer to the origin. Ph.D. Thesis, University of Utrecht, 1997.
- (155) Martins Alves, M. C.; Dodelet, J. P.; Guay, D.; Ladouceur, M.; Tourillon, G. *J. Phys. Chem.* **1992**, *96*, 10898.

CR020708R

